4694 J. Med. Chem. 2009, 52, 4694–4715
DOI: 10.1021/jm900259h

Journal of Medicinal Chemistry Article

Discovery of Leukotriene A4 Hydrolase Inhibitors Using Metabolomics Biased Fragment Crystallography†

Douglas R. Davies,‡ Bjorn Mamat,§ Olafur T. Magnusson,∥ Jeff Christensen,‡ Magnus H. Haraldsson,∥ Rama Mishra,§ Brian Pease,§ Erik Hansen,‡ Jasbir Singh,§ David Zembower,§ Hidong Kim,‡ Alex S. Kiselyov,§ Alex B. Burgin,‡ Mark E. Gurney,∥ and Lance J. Stewart*,‡

‡deCODE biostructures, Inc., 7869 NE Day Road West, Bainbridge Island, Washington 98110, §deCODE chemistry, Inc., 2501 Davey Road, Woodridge, Illinois 60517, and ∥deCODE genetics, Inc., Sturlugata 8, IS-101 Reykjavik, Iceland

Received March 2, 2009

We describe a novel fragment library termed fragments of life (FOL) for structure-based drug discovery. The FOL library includes natural small molecules of life, derivatives thereof, and biaryl protein architecture mimetics. The choice of fragments facilitates the interrogation of protein active sites, allosteric binding sites, and protein−protein interaction surfaces for fragment binding. We screened the FOL library against leukotriene A4 hydrolase (LTA4H) by X-ray crystallography. A diverse set of fragments including derivatives of resveratrol, nicotinamide, and indole were identified as efficient ligands for LTA4H. These fragments were elaborated in a small number of synthetic cycles into potent inhibitors of LTA4H representing multiple novel chemotypes for modulating leukotriene biosynthesis. Analysis of the fragment-bound structures also showed that the fragments comprehensively recapitulated key chemical features and binding modes of several reported LTA4H inhibitors.

Introduction

The wealth of data deposited by structural gnenomics initiatives indicates that ∼20% of protein crystal structures contain stably bound small molecules. These endogenous ligands include substrates, cofactors, products, bound metal ions,[1] and even components of the crystallant. For example, of ∼3500 structures deposited by the Protein Structure Initiative (as of January 2009), approximately 342 contain natural ligands and 280 contain cofactors (http://smb.slac.stanford.edu/jcsg/Ligand_Search/). Not infrequently, electron density deriving from an unknown ligand is present in deposited structures. Moreover, there are numerous reports of natural molecules that mediate powerful biological effects by stabilizing protein−protein interactions.[2,3] Evolution produced conserved protein motifs that optimally bind small molecules representing preferred or privileged chemical architectures. Kuntz et al.[4] showed empirically that for ligands that bind strongly to proteins, each non-hydrogen atom contributes about −1.5 kcal/mol to the free energy of ligand binding to about 15 non-hydrogen atoms (∼180 MW), the maximum size of most enzyme substrates or metabolites. Furthermore, the dominant interactions were van der Waals interactions that will depend upon shape complementarity and hydrophobic effects. Thus, the coevolution of protein structures with chemical architectures represented in the metabolome will select for optimization of van der Waals interactions based on shape complementarity. These preferred chemical architectures will bind proteins with high ligand efficiency. This suggests that the natural molecules of life represented by the metabolome[5] can be a preferred starting point for fragment based drug discovery (FBDD[a]).[6−8]

We therefore constructed a screening set for FBDD that we have called "fragments of life" (FOL). Fragment-based drug discovery has gained acceptance within the pharmaceutical industry (as reviewed by Congreve et al.[9]), as it provides an alternative to expensive and sometimes inefficient high-throughput screening (HTS) methods for chemical hit identification.[10] The general concept of FBDD involves screening of low molecular weight "rule of three" compounds (MW < 300, ≤3 rotatable bonds, ≤3 hydrogen bond donor/acceptor(s), TPSA < 60, ClogP < 3)[11] against target macromolecules using a variety of detection methods. These include X-ray crystallography, nuclear magnetic resonance (NMR), surface plasmon resonance, differential thermal denaturation, fluorescence polarization, and other techniques.[9,12−15]

† This manuscript describes structural information from 20 unique LTA4H structures with bound ligands, all of which have been entered into the Protein Data Bank and listed here in the following format (compound number bound to LTA4H,PDBID code): **2**, 3FTS; **3**, 3FTU; **3** + **1**, 3FTX; **4**, 3FTV; **4** + acetate, 3FTW; **5**, 3FTY; **6**, 3FU0; **7**, 3FU3; **8**, 3FU5; **9**, 3FU6; **10**, 3FUD; **11**, 3FUH; **12**, 3FUE; **13**, 3FUF; **14**, 3FUI; **15**, 3FUJ; **16**, 3FUK; **17**, 3FUM; **18**, 3FUN; **19**, 3FH7.

*To whom correspondence should be addressed. Phone: 206-780-8911. Fax: 206-780-8547. E-mail: lstewart@decode.com.

[a] Abbreviations: LTA4H, leukotriene A4 hydrolase; LCMS, liquid chromatography mass spectrometry; FOL, fragments of life; FBDD, fragment based drug discovery; TPSA, total polar surface area; NMR, nuclear magnetic resonance; PDB ID, Protein Data Bank identification number; ClogP, calculated log of octanol/water partition coefficient; LTB4, leukotriene B4; FOL-Nat, members of the fragments of life library that are natural molecules of life; FOL-NatD, members of the fragments of life library that are synthetic derivatives or isosteres of natural molecules of life; FOL-Biaryl, members of the fragments of life library that are synthetic biaryl molecules, many of whose energy minimized structures mimic α-, β-, and γ-turns; HWB, human whole blood; rt, room temperature.

 Published on Web 07/20/2009

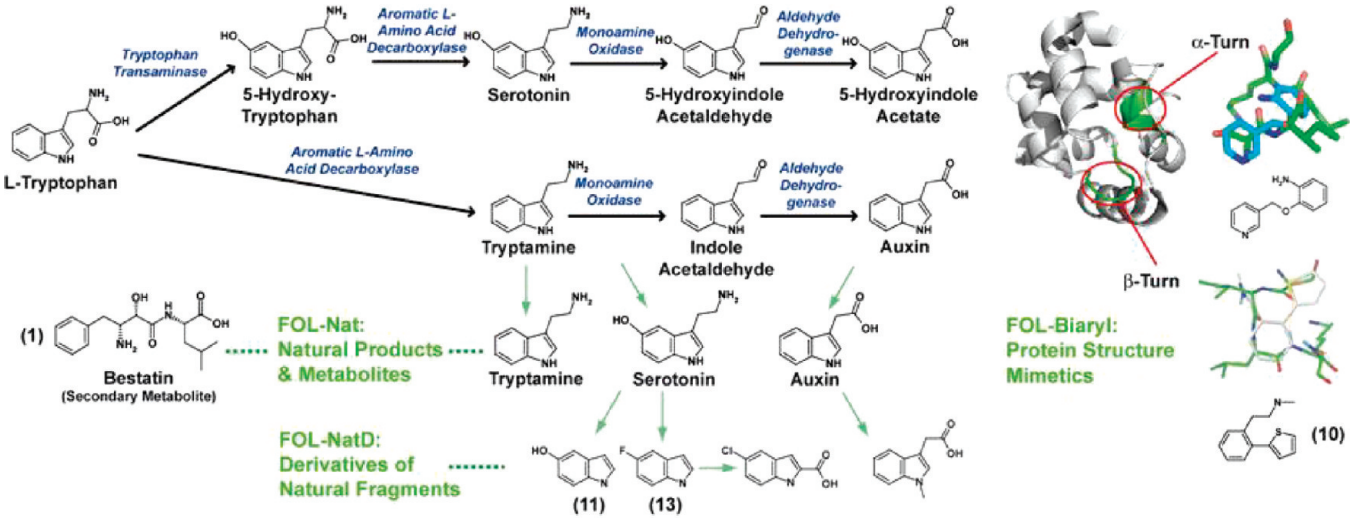

Figure 1. Conceptual organization of key components of the fragments of life library, with example fragments. The current FOL library (1329 molecules) contains chemically tractable natural small molecule metabolites such as bestatin **1** (FOL-Nat), metabolite-like compounds and their bioisosteres (FOL-NatD), and protein architecture mimetics (FOL-Biaryl). Any natural molecule with MW $<$ 350 Da that exists as a substrate, natural product, or allosteric regulator of any metabolic pathway in any cell type is a potential candidate FOL-Nat fragment. Example fragments **11** and **13** that contain the privileged scaffold indole[98] from the serotonin and auxin biosynthetic pathways are shown. FOL-NatD fragments are defined as heteroatom containing derivatives, analogues, or fragments of any FOL-Nat molecule. FOL-Biaryl fragments were selected from a variety of biaryl compounds that are potential mimics of protein α, β, or γ turns.[59−61] At the right-hand side of the figure, compound **10** can be seen superimposed on a β-turn of a protein structure (residues Ala20-Ala21-Asp22-Ser23 of PDB ID 1RTP). An additional FOL-Biaryl component is also shown, superimposed on an α-turn (residues Ser65-Ile66-Leu67-Lys68 of PDB ID 1RTP).

The design of reasonably sized fragment libraries is essential for successful FBDD. Considering both the concepts of ligand efficiency[16] and the size of feasible chemical space for fragments,[17] we strived to establish a compact fragment set (~1300 molecules) that (i) encompasses diverse biological and chemical thought, (ii) facilitates chemical optimization, and (iii) has solubility properties that make the library compatible with rapid screening methods (Figure 1). We selected this library size reasoning that at least half of the marketed drug molecules can be constructed from a limited set of privileged structures.[18−21] In assembling the fragment set, we also took note of independent research findings on the origin of conserved metabolism,[22] ligand−protein binding data from international structural genomics efforts,[23] and scaffold framework diversity calculations for organic molecules.[24]

To determine the utility of the FOL library, it was screened against leukotriene A4 hydrolase (LTA4H) by X-ray crystallography. LTA4H is a 69 kDa bifunctional enzyme with aminopeptidase and epoxide hydrolase activities that utilize a single zinc active site.[25−27] The leukotrienes are a group of proinflammatory lipid mediators that have been implicated in the pathogenesis and progression of atherosclerosis.[28] For example, it has been shown that a haplotype (HapK) spanning the LTA4H gene confers an increased risk of myocardial infarction,[29] a finding that is consistent with a growing body of biochemical and cell biological research.[30] Single nucleotide polymorphisms spanning the LTA4H gene have also been correlated with increased risk of asthma and allergy susceptibility.[31] The importance of LTA4H as a therapeutic target is exemplified by the development of multiple inhibitors representing different chemotypes.[32−43]

The active site pocket of LTA4H is a 17 Å long L-shaped cleft capable of binding the leukotriene A4 substrate. The crystal structure of LTA4H[26] was originally solved bound to bestatin (**1**), a low molecular weight secondary metabolite of *Streptomyces olivoreticuli*[44] and a component of the FOL library. The catalytic domain of LTA4H shares a high degree of structural similarity with the metalloprotease thermolysin including a conserved active site zinc binding motif (HEXXH-X18-E) (Figure 2A). Very little is known about the biological relevance of the LTA4H aminopeptidase activity. It is speculated that the enzyme may process peptides related to inflammation and host defense.[45,46] As a hydrolase, the enzyme converts the oxirane ring of LTA4 to the respective diol, leukotriene B4 (LTB4), which acts as a chemoattractant and an activator of inflammatory responses mediated by binding to G-protein-coupled receptors BLT1 and BLT2.[47−51]

In this report we show that the FOL library yielded fragment hits including natural molecules such as resveratrol and derivatives of nicotinamide. We also show how FOL hits could be elaborated into potent LTA4H inhibitors with drug-like properties representing novel chemotypes. These fragment-based inhibitors show good ligand efficiency for inhibition of peptidase and hydrolase activities in vitro.

Results

FOL Library Design. In order to facilitate use of the FOL library in a diverse set of applications, each of its members was determined to have solubility in methanol at greater than 50 mM (see Materials and Methods). Individual members of the FOL library were maintained as 50 mM stocks in methanol which allowed them to be dispensed and dried into powders for subsequent dissolution into new formulations with no residual solvent (e.g., crystal soaking conditions). Within the FOL library, we defined natural molecules of life "FOL-Nat" to be any small molecule (MW $\lesssim$ 350) which is known to be produced by any living organism and therefore represented within the metabolome.[5] Without bias for any particular metabolic pathway, the current FOL-Nat set includes 218 molecules of life. It is noteworthy that the first LTA4H crystal structure was obtained with bestatin **1**, a natural metabolite bound in the active site, and there are

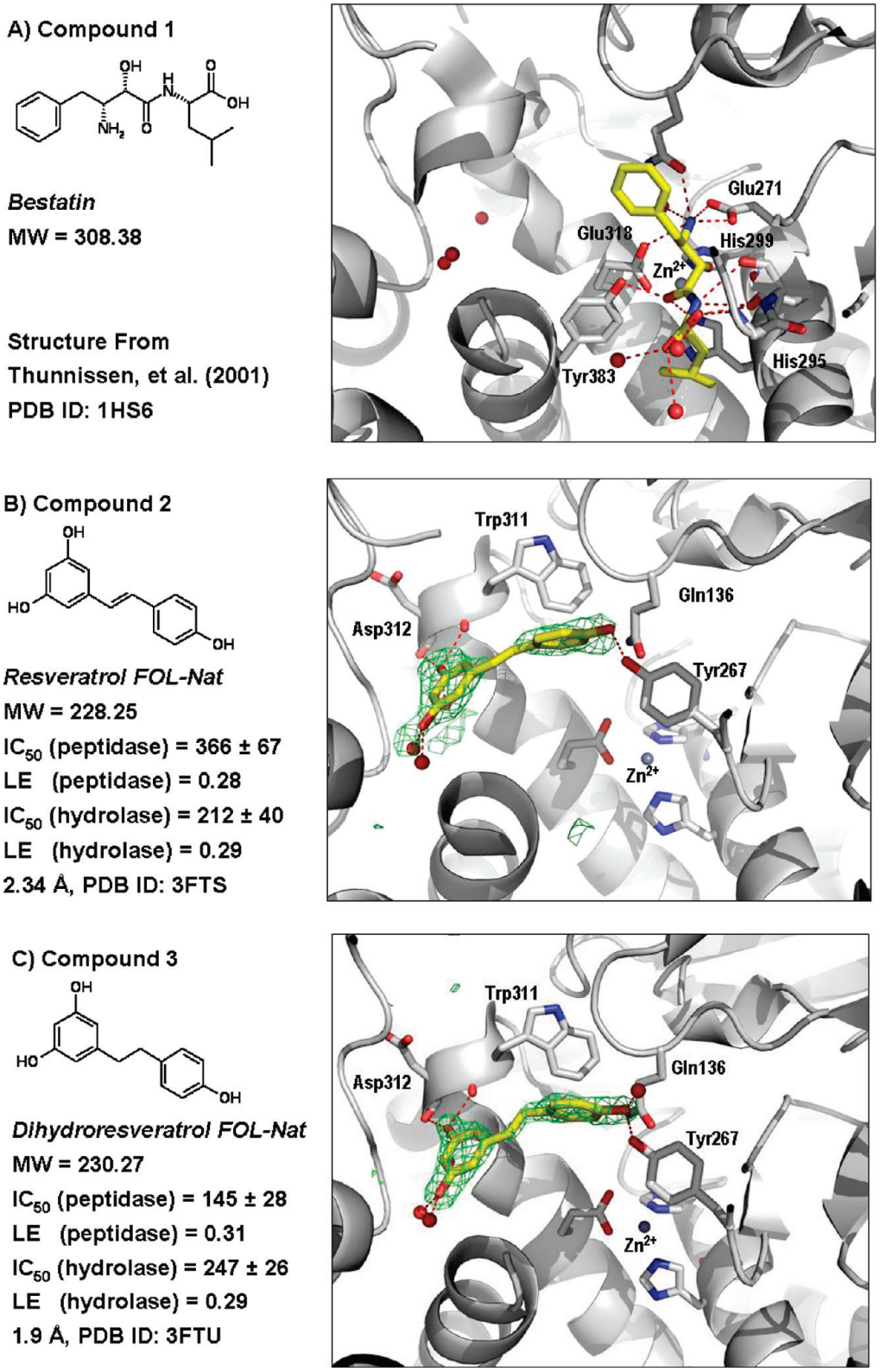

Figure 2. Continued

numerous similar examples of natural molecules leading to the design of drug candidates that modulate protein activity.[52−54] Evolutionary concepts of substrate ambiguity and enzyme promiscuity suggest that many enzyme active sites have evolved flexibility to transiently bind substrates and products.[55−58] We therefore decided to add heteroatom derivatives and isosteres of natural molecules of life to our fragment set. Termed "FOL-NatD", these synthetic derivatives or isosteres of natural molecules of life are anticipated to be fortified with small modifications that could stabilize binding to enzyme active sites. The current FOL-NatD set includes 666 fragments. In order to emulate 3D protein architecture and to further diversify the FOL library, we have included a set of 445 synthetic biaryl molecules, many of

D) Compound 4

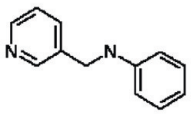

FOL-NatD
MW = 184.24
IC_{50} (peptidase) = 1321 ± 257
LE (peptidase) = 0.28
IC_{50} (hydrolase) = 1667 ± 168
LE (hydrolase) = 0.27
1.7 Å, PDB ID: 3FTV

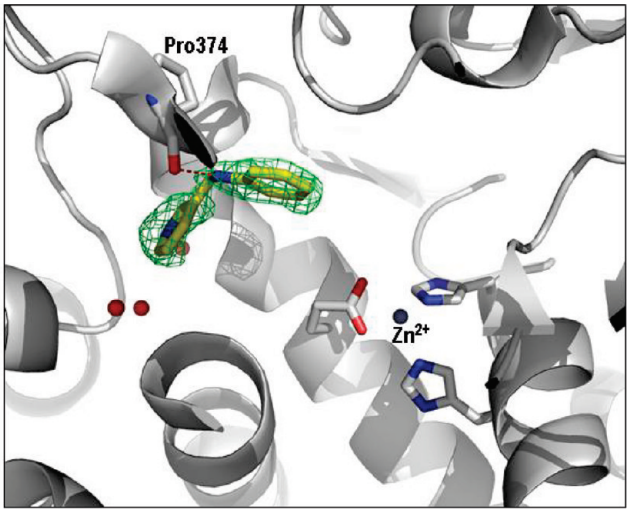

E) Compound 5

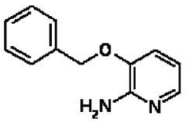

FOL-NatD
MW = 200.24
IC_{50} (peptidase) = 308 ± 39
LE (peptidase) = 0.32
IC_{50} (hydrolase) = 619 ± 131
LE (hydrolase) = 0.29
2.15 Å, PDB ID: 3FTY

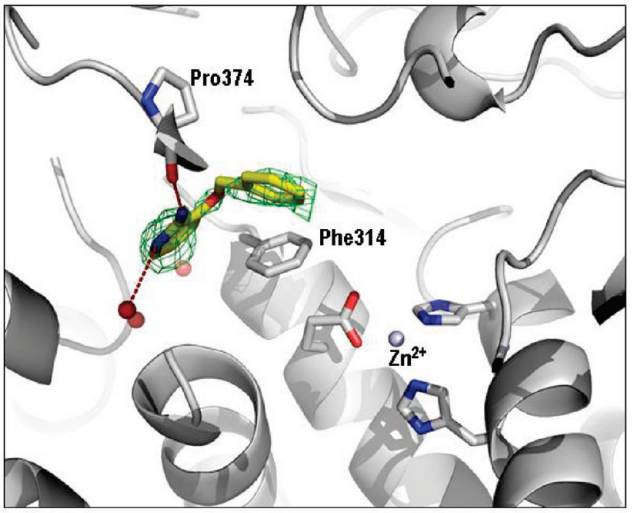

F) Compound 6

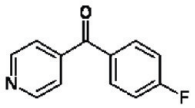

FOL-NatD
MW = 201.20
IC_{50} (peptidase) = 3673 ± 153
LE (peptidase) = 0.22
IC_{50} (hydrolase) = 5308
LE (hydrolase) = 0.21
1.8 Å, PDB ID: 3FU0

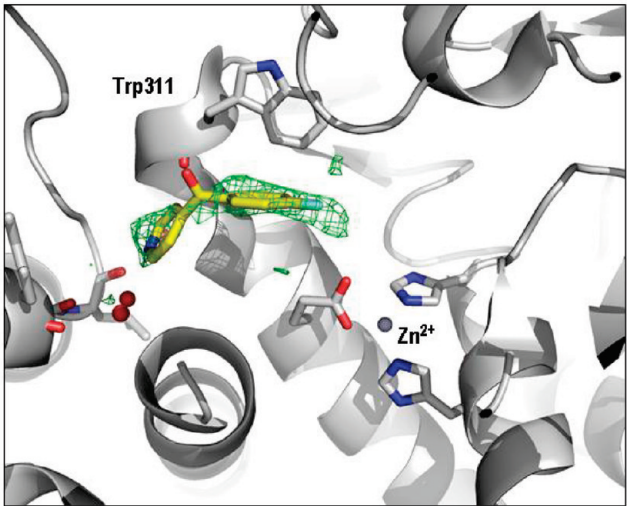

Figure 2. Continued

whose energy minimized structures mimic α-, *β*-, and *γ*-turns.[59−61] This subset of the FOL library was named "FOL-Biaryl." All of the listed FOL concepts are summarized in Figure 1.

Our final 1329 member FOL library generally conforms to the "rule of three" guidelines for fragments[11] (see Supporting Information Figure 1 for physical and chemical properties of the FOL library) and contains approximately 400 distinct chemotypes (see Supporting Information Figure 2 for calculated diversity properties of the FOL library). Members of the complete FOL library have an average molecular weight of 182.5, ClogP of 0.96, 1.49 hydrogen bond donors, 2.56

G) Compound 7

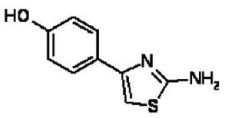

FOL-NatD
MW = 192.24
IC_{50} (peptidase) = >1000
LE (peptidase) =
IC_{50} (hydrolase) = 1443 ± 63
LE (hydrolase) = 0.30
2.0 Å, PDB ID: 3FU3

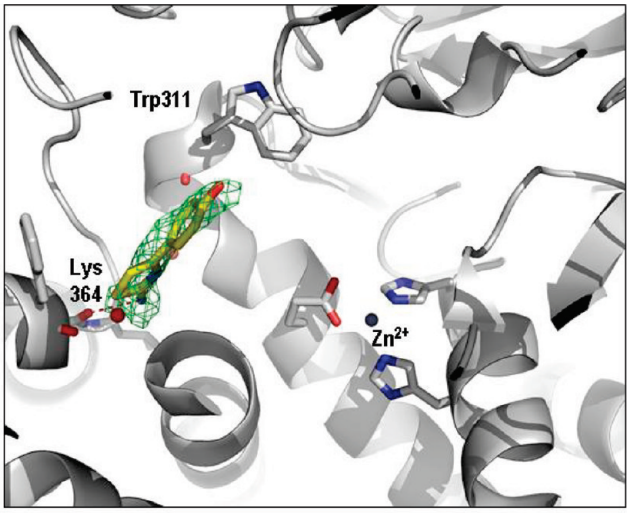

H) Compound 8

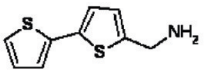

FOL-NatD
MW = 195.31
IC_{50} (peptidase) = 38.9 ± 15.9
LE (peptidase) = 0.50
IC_{50} (hydrolase) = 75.2 ± 7.3
LE (hydrolase) = 0.47
2.3 Å, PDB ID: 3FU5

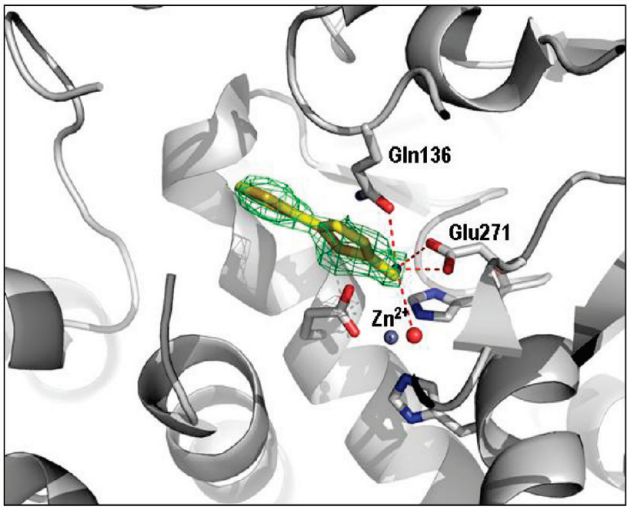

I) Compound 9

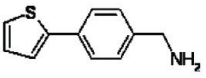

FOL-NatD
MW = 189.28
IC_{50} (peptidase) = 106 ± 23
LE (peptidase) = 0.42
IC_{50} (hydrolase) = 106 ± 20
LE (hydrolase) = 0.42
2.05 Å, PDB ID: 3FU6

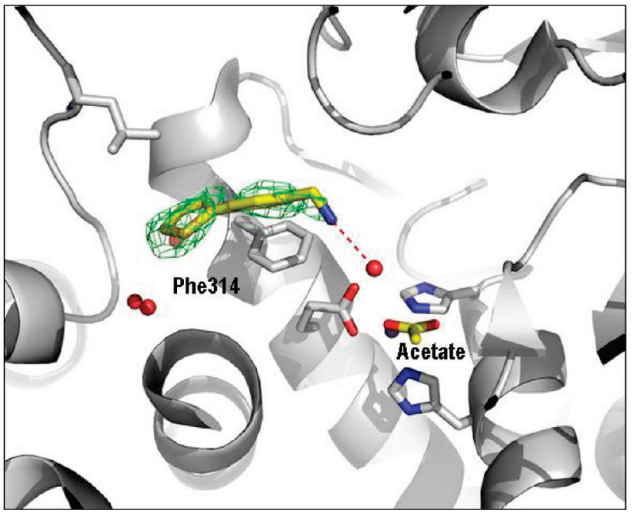

Figure 2. Continued

hydrogen bond acceptors, 1.7 rings, and 2.7 rotatable bonds. The only parameter that lies outside the rule of three is polar surface area with an average value of 118.9 $Å^3$. This is reflective of the water-soluble properties of many small molecules of life. We reasoned that members of the FOL library represent "molecular rulers" providing information on the architecture and electronics of protein binding sites. Thus, our FOL library is designed to interrogate both enzyme active sites along with the more intriguing opportunities to probe allosteric pockets and protein−protein interaction surfaces.

LTA4H Target FOL Screening. To validate the FOL library as a screening set in a proof of concept study,

J) Compound 10

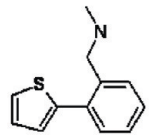

FOL-NatD, surface binder
MW = 203.31
IC_{50} (peptidase) = 1077 ± 59
LE (peptidase) = 0.29
IC_{50} (hydrolase) = >2000
LE (hydrolase) = n/d
2.2 Å, PDB ID: 3FUD

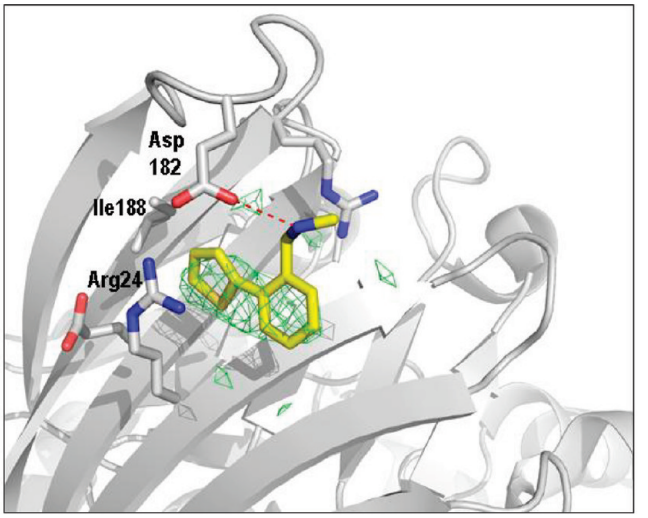

K) Compound 11

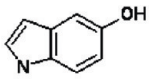

FOL-NatD
MW = 133.15
IC_{50} (peptidase) = >1000
LE (peptidase) = --
IC_{50} (hydrolase) = >2000
LE (hydrolase) = --
1.8 Å, PDB ID: 3FUH

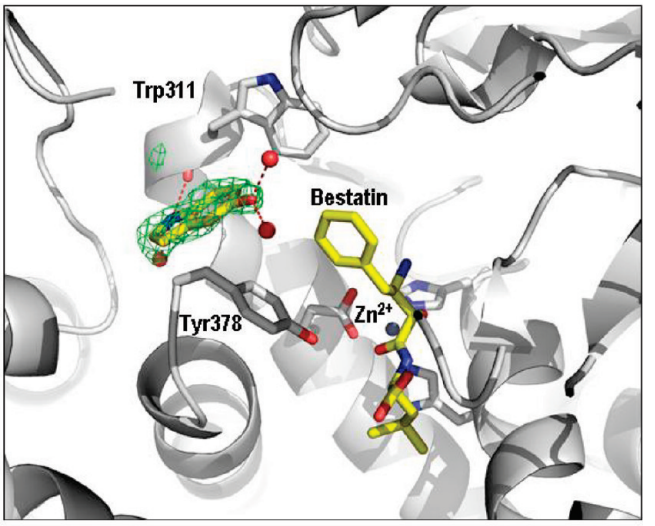

L) Compound 12

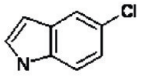

FOL-NatD
MW = 151.60
IC_{50} (peptidase) = > 1000
LE (peptidase) = --
IC_{50} (hydrolase) = 1510 ± 139
LE (hydrolase) = 0.38
2.4 Å, PDB ID: 3FUE

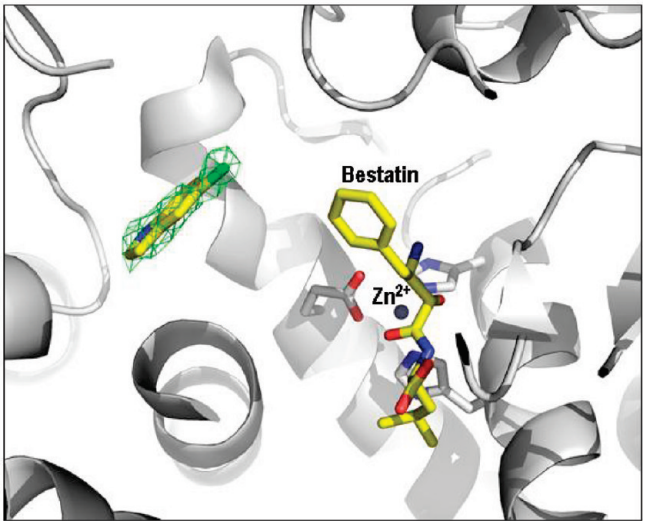

Figure 2. Continued

approximately 15% of the fragments were screened against LTA4H by soaking respective crystals with randomly selected pools each containing eight different structurally diverse FOL fragments (see details of Computational and Physical Pooling in Materials and Methods). The resulting crystals were frozen, complete X-ray diffraction data sets were collected, and the models were partially refined using an LTA4H protein-only model. When unaccounted electron density was observed, candidate fragments from the pool that were consistent with the shape of the density were soaked individually and additional complete data sets were collected. When definitive electron density from a single

M) Compound 13

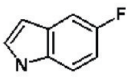

FOL-NatD
MW = 135.14
IC_{50} (peptidase) = >1000
LE (peptidase) = --
IC_{50} (hydrolase) = >2000
LE (hydrolase) = --
2.6 Å, PDB ID: 3FUF

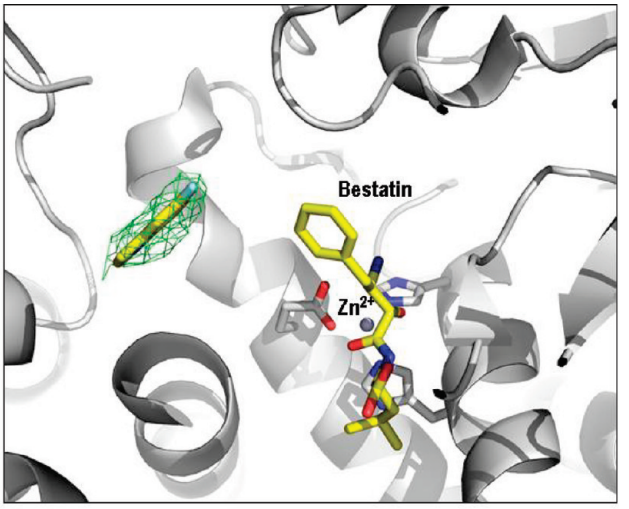

N) Compound 14

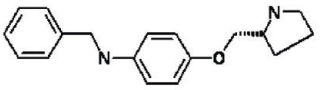

Elaboration of (4)
MW = 282.39
IC_{50} (peptidase) = 0.207 ± 0.05
LE (peptidase) = 0.43
IC_{50} (hydrolase) = 0.157 ± 0.03
LE (hydrolase) = 0.44
IC_{50} (HWB) = 0.131 ± 0.057
LE (HWB) = 0.45
2.2 Å, PDB ID: 3FUI

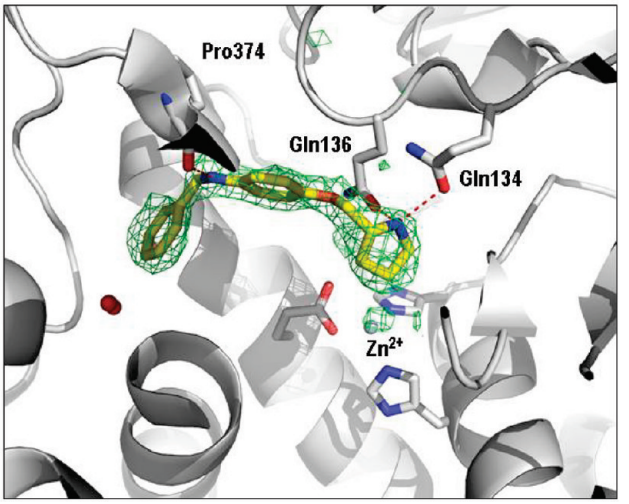

O) Compound 15

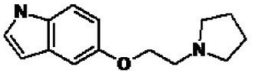

Elaboration of (11)
MW = 230.31
IC_{50} (peptidase) = 321 ± 44
LE (peptidase) = 0.28
IC_{50} (hydrolase) = 234 ± 21
LE (hydrolase) = 0.29
1.9 Å, PDB ID: 3FUJ

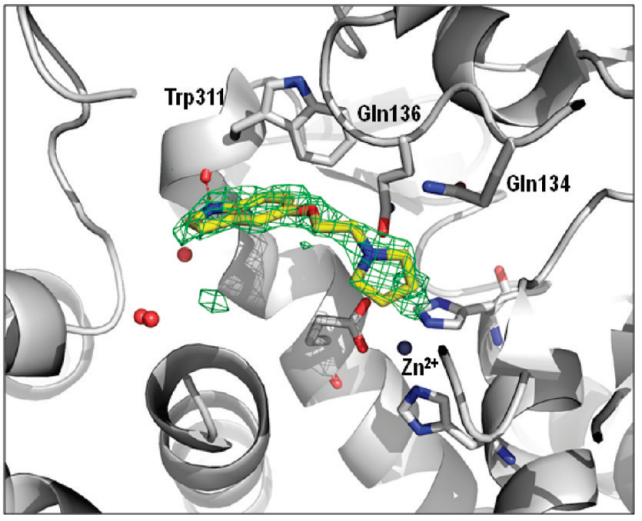

Figure 2. Continued

compound soak was observed, the fragment was built into the electron density and the complete protein−fragment model was refined. Thirteen unique hits were identified from these experiments, 12 of which are summarized in Figure 2B−M, representing an overall hit rate of 6%. The 13th fragment, an FOL-Biaryl member, will be described in a separate publication.[43] Crystallographic data collection and refinement statistics for all structures are listed in Supporting Information Table 1. LTA4H inhibition assay data for all compounds in this manuscript are listed in Supporting Information Table 2 and are also summarized in Figure 2.

P) Compound 16

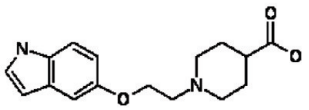

Elaboration of (11)
MW = 288.35
IC_{50} (peptidase) = 1491 ± 291
LE (peptidase) = 0.18
IC_{50} (hydrolase) = 966 ± 322
LE (hydrolase) = 0.20
1.95 Å, PDB ID: 3FUK

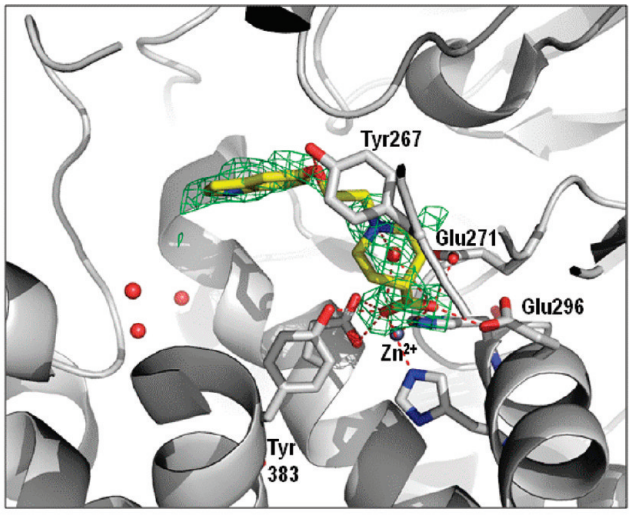

Q) Compound 17

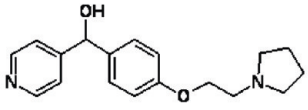

Elaboration of (6)
MW = 298.39
IC_{50} (peptidase) = 202 ± 17
LE (peptidase) = 0.23
IC_{50} (hydrolase) = 170 ± 5
LE (hydrolase) = 0.23
2.15 Å, PDB ID: 3FUM

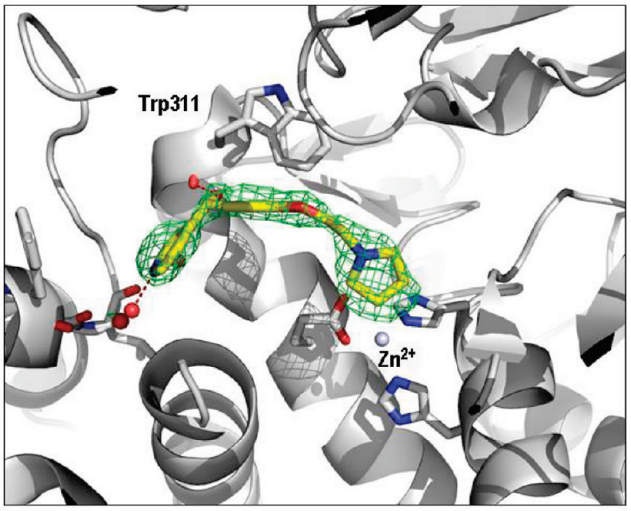

R) Compound 18

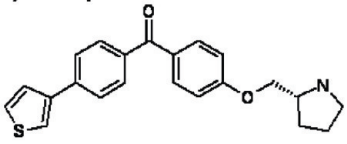

Elaboration of (6)
MW = 363.48
IC_{50} (peptidase) = 0.081 ± 0.02
LE (peptidase) = 0.37
IC_{50} (hydrolase) = 0.189 ± 0.02
LE (hydrolase) = 0.35
IC_{50}(HWB) = 4.58 ± 1.33
LE (HWB) = 0.27
1.58 Å, PDB ID: 3FUN

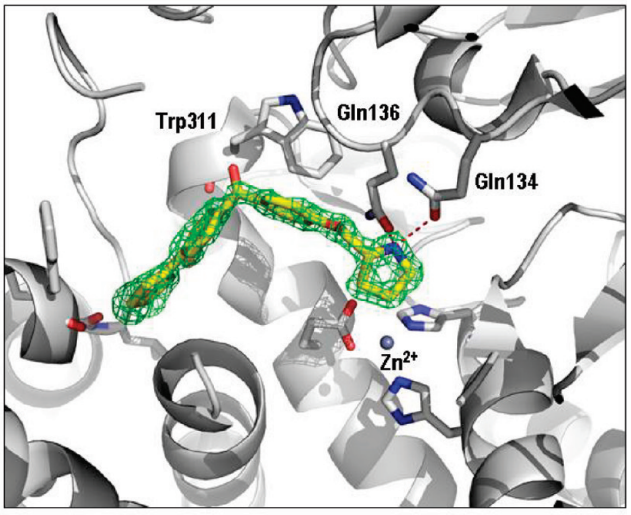

Figure 2. Continued

Representative fragments from all categories of FOL were observed bound to LTA4H (FOL-Nat, FOL-NatD, and FOL-Biaryl). Nine of the 13 FOL hit compounds were discovered to bind independently within the L-shaped substrate binding cleft. The FOL-Biaryl compound **10** was found to bind on the surface of LTA4H, far from the active site. Compound **7** was simultaneously bound to both the surface and within the L-shaped cleft of LTA4H (see Supporting Information Figure 3, an image of LTA4H surface binding of **7**). Three additional FOL-NatD molecules (**11**−**13**) were accommodated in the substrate binding cleft only upon concomitant binding of an additional inhibitor,

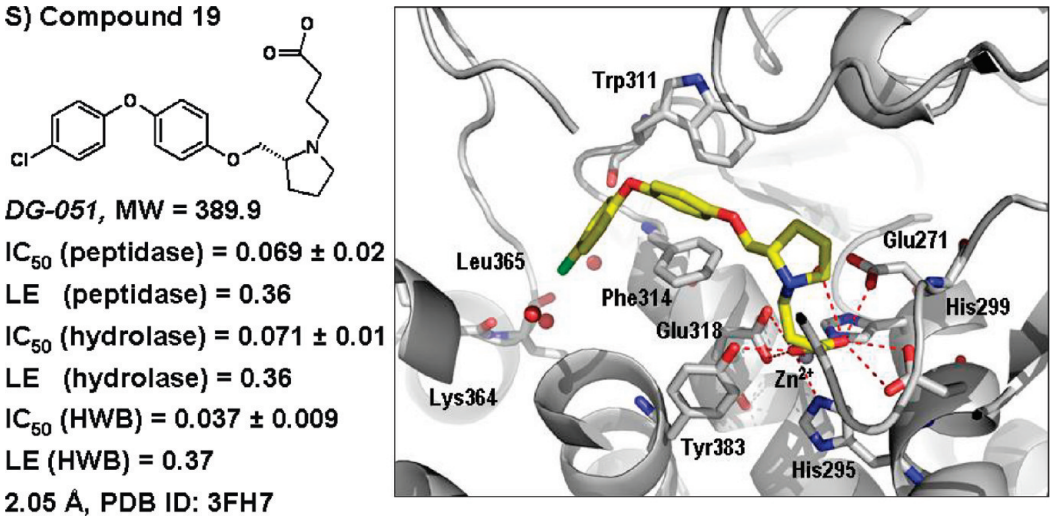

Figure 2. Panels showing ligand binding to LTA4H for compounds described in the manuscript. Enzyme assay IC_{50} values are in μM, human whole blood cell assay IC_{50} values are in nM when reported, and ligand efficiency (LE) values are in kcal/(mol·heavy atom). Compound structures are displayed as yellow stick structures, and LTA4H is displayed in gray. Green mesh corresponds to the $F_o - F_c$ (difference) electron density at the 3.0σ level of the crystal structure with the compound omitted from the model. Polar contacts with LTA4H and/or bound water molecules are shown as red dashed lines. PDB IDs for each structure are indicated.

bestatin (**1**). The binding modes of individual fragments are briefly described below.

The natural product resveratrol (compound **2**),[62,63] a plant-derived polyphenol, was identified as a hit in our screen (Figure 2B). This natural molecule has been implicated in cardioprotection and antiaging.[64−70] The polyphenol nature of **2** suggests that it could make multiple hydrogen bonds with the target including conserved water molecules at the bottom of the cleft and the backbone carbonyl of Gln136. In our hands, **2** was a relatively weak binder of LTA4H with IC_{50} values of 366 and 212 μM in the peptidase and hydrolase assays, respectively. The observed electron density for the molecule was of intermediate quality. The model of the bound fragment in the crystal structure refined with relatively high temperature factors. Analysis of the structure of the resveratrol complex further suggested that the bound compound exists in a strained conformation due to the rigid C7−C8 double bond. From this observation, we postulated that dihydroresveratrol (compound **3**), a major metabolite of **2** observed in mammals,[64,71,72] would have more rotational freedom and may bind more effectively to LTA4H. We synthesized **3** and soaked LTA4H protein-only crystals. The resulting crystal structure showed very clear electron density for **3**, and the fully refined model exhibited lower relative temperature factors compared to **2** (Figure 2C). Specifically, bound **3** displayed a conformation inaccessible to **2**, with a torsion angle of −161.2° around the C7−C8 bond (Figure 3A). The observed better fit of **3** for binding LTA4H did not translate to an increase in binding affinity, possibly because of an energetic trade-off between an improved fit and an entropic penalty to be paid by constraining a more flexible ligand. The IC_{50} of **3** was comparable to that of the parent resveratrol **2**: 145 μM in the peptidase assay and 247 μM in the hydrolase assay.

N-(Pyridin-3-ylmethyl)aniline **4** is classified as an FOL-NatD fragment. It shares structural similarities with nicotinamide, namely, a pyridin-3-carboxamide moiety. It was bound at the bottom of the substrate binding cleft of LTA4H near the resveratrol binding site (Figure 2D). Most interactions of **4** with the protein were hydrophobic except for a potential hydrogen bond between the aniline *N*H and the backbone carbonyl of Pro374. Compound **4** displayed IC_{50} values of 1.32 and 1.67 mM in the peptidase and hydrolase assays, respectively. Notably, **4** displayed structural similarity compared to the phenoxymethylbenzene pharmacophore of the previously reported inhibitors of LTA4H[40] (PDB IDs 3CHO, 3CHQ). Superposition of 3CHQ or 3CHO structures with our LTA4H-**3** and LTA4H-**4** complexes demonstrated that the corresponding atoms of the phenoxymethylbenzene were all within 0.7 Å of their counterparts in **3** or **4** (see Supporting Information Figure 4). The structurally related fragment 3-(phenylmethoxy)pyridin-2-amine (**5**) identified in our screen featured a similar binding mode (Figure 2E). The 2-amino function of the pyridine ring is likely to mediate a potential 2.8 Å hydrogen bond with the backbone carbonyl of Pro374. This bond is shorter and has more favorable geometry compared to that between **4** and Pro374. Notably, the interaction between the amine and Pro374 moiety slightly perturbed the binding pose of the biaryl scaffold. Better binding interactions of **5** with the target translated into its better potency (IC_{50} values of 308 and 619 μM in peptidase and hydrolase assays). It is noteworthy that the hydroxamic acid inhibitors of LTA4H, which also contain phenoxymethylbenzene, do not appear to occupy similar space in LTA4H, most likely because of the dominant interactions that the hydroxamic acid component has with the catalytic zinc ion[73] (see Supporting Information Figure 4).

We categorized the pyridine analogue **6** as an FOL-NatD molecule. It features a pyridine ring present in several molecules of life including niacin, vitamin B_3 (pyridine-3-carboxylic acid), and 4-pyridoxic acid, the catabolic breakdown product of vitamin B_6. In our studies, fragment **6** was bound to the hydrophobic center of the LTA4H cleft, in the same location as **4**. The carbonyl oxygen of **6** was in a suboptimal position, namely, within 3.6 Å of the carbonyl oxygen of Trp311 (Figure 2F). This unfavorable interaction likely contributed to poor activity of the fragment in the biological assays (IC_{50} = 3.7 and 5.3 mM in peptidase and hydrolase assays, respectively).

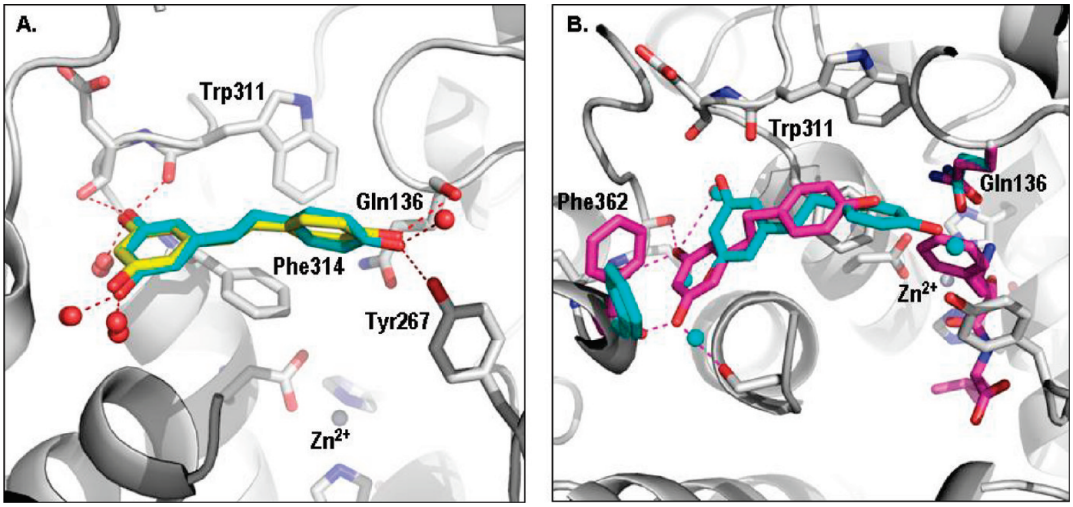

Figure 3. Resveratrol structures. (A) The structure of resveratrol (**2**) (yellow) is superimposed upon dihydroresveratrol (**3**) (cyan). (B) Superposition of the structure of dihydroresveratrol (**3**) is shown in the absence (cyan) and presence (magenta) of bestatin. Structurally conserved water molecules and the side chain of residue Phe362 are also color-coded to show the differences in the structures with and without bestatin. For crystallographic data, see Supporting Information Table 1.

Two additional FOL-NatD fragment hits (compounds **7** and **9**, Figure 2G and Figure 2I) and two FOL-Biaryls (compounds **8** and **10**, Figure 2H and Figure 2J) featured thiazole (a component of thiamine, vitamin B_1) or thiophene rings. Although several thiazole derivatives have been identified as promiscuous protein binders,[74] this chemotype provided valuable structural insight into LTA4H. Specifically, molecules **7**−**9** displayed distinctly different binding modes to the enzyme. They mapped out space occupancy of the entire L-shaped substrate cavity of LTA4H (see Supporting Information Figure 5). For example, **7** was bound deep within the LTA4H cavity (Figure 2G). The aminothiazole group displaced two of the three structurally conserved water molecules at the bottom of the substrate binding cleft. The amino substituent of the thiazole group occupied a position roughly between binding sites of the two displaced water molecules and was within hydrogen bonding distance of the carbonyl oxygen of Phe362. Thiophene derivative **8** was bound at the other end of the LTA4H substrate binding cleft near the zinc binding site (Figure 2H). The primary amino group of the fragment was less than 4 Å from the zinc atom, 2.9 Å from Oε1 of Gln136, and 2.7 Å from a carboxyl oxygen of Glu271. Finally, the binding site of **9** was intermediate between **7** and **8**, with the thiophene ring making hydrophobic contact with Phe314 and Leu369 (Figure 2I). The amino group of **9** did not make any hydrogen bonds with LTA4H. The thiophene ring did not displace the structurally conserved water molecules, as was observed for **8**. Both **8** and **9** were relatively potent ligands of LTA4H with measured IC_{50} values equal to or below 100 μM in both peptidase and hydrolase assays. Compound **7** afforded poor inhibitory activity with IC_{50} values greater than 1 mM. This could be a result of its binding mode being deep within the substrate binding cleft, perhaps making it unable to interfere with substrate binding in either of our LTA4H enzyme assays. Interestingly, a second molecule of **7** appeared to be bound in the LTA4H−**7** cocrystal complex on the surface of the protein. Its phenol moiety was in position to make polar contact with the carboxyl side chain of Glu501 and the backbone carbonyl of Leu343 (see Supporting Information Figure 3). This molecule was also well situated to make polar contact with imidazole bound between Glu501 and Glu348. Imidazole is present in the crystallization buffer and is included in most LTA4H structures observed at medium or higher resolution.

Of all the fragments identified by crystallographic screening, only compound **10** (FOL-Biaryl) did not bind in the substrate binding cavity (Figure 2J). It interacted with the surface of the protein, in a pocket formed by Arg24, Ile188, and Asp182. We have further confirmed the LTA4H binding of **10** and **7** (which binds a different pocket on the surface of LTA4H) by both surface plasmon resonance and saturation transfer difference NMR studies[75] (data not shown). Molecule **10** was not competitive with bestatin (**1**) an LTA4H competitive inhibitor (data not shown) and displayed little or no inhibitory activity against LTA4H (IC_{50} > 1 mM). Therefore, the two shallow surface pockets mapped out by compounds **10** and **7** are unlikely to be useful targets for inhibition of LTA4H. However, our findings suggest that the application of FOL methodology may yield additional insight into the topology of surface domains or allosteric sites. It could be further used to develop modulators of protein−protein interactions.[76]

Simultaneous LTA4H Binding of Two Fragments. The two most common approaches in FBDD are fragment evolution and fragment linking.[9] The fragment evolution technique involves chemical optimization of the initial fragment hit to produce higher affinity ligands.[77] Fragment linking is focused on assembling adjacent independently bound fragments into a single molecule to produce high affinity ligands.[78−81] In order to expedite the transition from fragment hits to leadlike molecules, we explored the possibility of identifying dual simultaneous FOL hits in LTA4H. This "fragment plus fragment" approach was inspired by a growing number of cases where two small molecules bind within protein targets and contact each other. For example, this can be seen in the interaction of the plant hormone auxin (indole-3-acetic acid)[82] and an inositol hexakisphosphate cofactor in the crystal structure of the TIR1-ASK1 complex.[2]

In one "fragment plus fragment" approach, we soaked LTA4H crystals with FOL pools that were spiked with 1 mM bestatin (IC_{50} = 178 nM in peptidase assay). Subsequent

screening of FOL yielded three different indole fragments (compounds **11**−**13**) bound in the substrate binding cleft (Figure 2K−M). Notably, these fragments interacted with LTA4H only in the presence of bestatin. A representative example, 5-hydroxyindole (compound **11**) was a component of the FOL-NatD subset. This core is exhibited in the 5-hydroxyindole-3-acetic acid structure, which is a serotonin metabolite[83] (Figure 1). It was bound near residues Trp311 and Tyr378, with the hydroxyl oriented closest to the bestatin, 3.5 Å away (Figure 2K). Two halogenated analogues of **11**, namely, **12** and **13** lined up with the target in a similar orientation. Both chlorine and fluorine atoms of **12** and **13**, respectively, were ∼5.7 Å away from the nearest atom of the phenyl ring of bestatin. The shift in the binding mode of these indoles likely results from their decreased polar surface area compared to **11**. All obtained X-ray structures revealed well-defined electron density maps for bestatin with a binding mode essentially identical to that previously observed.[26]

In another approach, we sought to determine if the presence of bestatin could alter the binding mode of another fragment hit whose binding pose would be expected to be overlapping or incompatible with bestatin. Our rationale for this approach was to determine if the binding mode(s) of any fragments could be adjusted by induced-fit mechanisms resulting from the bestatin interaction with Zn^{2+}. With this approach, we found that bestatin could induce dihydroresveratrol (**3**) to adopt a different pose compared to the fragment **3** alone within the LTA4H substrate binding cavity (Figure 3A). Specifically, a brief LTA4H crystal soak of **3** (25 mM) followed by a 4 h soak with a mixture of **3** (25 mM) and bestatin (1 mM) resulted in a structure where **3** was displaced by ∼2.5 Å from its original binding site. With bestatin chelating the Zn^{2+} in its typical binding mode, molecule **3** was forced to bind at the bottom of the LTA4H substrate binding cleft. It displaced two of the three structurally conserved water molecules with its phenolic hydroxyl groups (Figure 3B) and was within a distance of ∼3.3 Å to bestatin. The torsional angle about the C7−C8 bond featured by the molecule in a LTA4H−**3**−bestatin structure was approximately 169°. Resveratrol (compound **2**) could not be visualized in a similar crystal cosoak with bestatin. We attributed this outcome to the lack of flexibility in **2** that is critical to the binding at the bottom of the binding cleft in the presence of bestatin. The discovery of a binding mode unattainable without a second fragment was an interesting outcome from the "fragment plus fragment" approach. In this case, bestatin altered the topology of LTA4H binding cavity and pushed dihydroresveratrol deeper into the cavity. As a result, the molecule adopted a novel binding mode requiring the side chain movement of Phe362. The new observed binding mode is intriguing, particularly in the displacement of structurally conserved waters. It is conceivable that fragment elaboration principles could be employed to produce potent inhibitor(s) that incorporates design concepts of both bestatin and the novel dihydroresveratrol interaction.

Acetate is one of the smallest of fragments, with just four non-hydrogen atoms and a molecular weight of 56. In LTA4H, acetate ions in the crystallization solution were often visualized binding to Yb^{3+} ions that are located at a key crystal lattice interface.[26,27,73] Similarly, we have observed acetate binding to the catalytic Zn^{2+} in the high resolution crystal structures of LTA4H with FOL compound **9** (Figure 2I). We sought to extend the "fragment plus fragment" strategy by employing acetate bound at the catalytic zinc in combination with other fragments. Notably, when 200 mM acetate was included as an additive in an LTA4H crystal soak with compound **4**, the final solved structure revealed both acetate and compound **4** binding simultaneously as anticipated from their previously observed individual binding modes. It is interesting to note that the acetate−Zn^{2+} binding events together with the binding modes of compounds **4**, **5**, and **9** were essentially superimposable (see Supporting Information Figure 6). On the basis of this observation, we postulated that a proper linking of carboxylic acid functionality to a hydrophobic biaryl would yield a potent inhibitor. Of particular interest were templates that could provide for the proper dihedral angle and distances in positioning both biaryl and acetate pharmacophores within the active site of LTA4H. Physicochemical properties, good ligand efficiency, and chemical feasibility were additional criteria we considered. In the course of chemical studies, (*R*)-prolinol was selected as a tether between a hydrophobic biaryl and a metal-binding carboxylate, yielding DG-051 (**19**), a drug molecule that has completed phase IIa clinical studies.[43] Thus, the DG-051 molecule (Figure 2S) displays two key pharmacophore features suggested by our fragment-based studies, namely, a carboxylic acid moiety binding to the active site zinc and a hydrophobic anchor at the bottom of the substrate binding cavity.

Elaboration of FOL Fragment Hits. The abundance of fragment screening data summarized above prompted us to improve the potency of several FOL hits through a limited medicinal chemistry effort. The rationale was to conceptually prove that the identified weak binders could be rapidly evolved into a potent LTA4H inhibitors following structural guidance obtained thus far. On the basis of the synthetic feasibility, we selected three fragments (**4**, **6**, and **11**) as templates for this chemical elaboration (see Schemes 1−3). In selecting proper pharmacophores for our chemistry effort, we considered both the trajectory for fragment linkage as suggested by the structural studies as well as druglike character of the designed molecules. Midsized cyclic amines were of particular interest, as they offered well-defined spatial orientation for the pharmacophores. Furthermore, these moieties were expected to mediate additional interaction within the active site and to enhance solubility and permeability of a fragment derivative across biological barriers. A brief synthetic effort followed by crystallographic screening converged on (*R*)-prolinol as a suitable tertiary amine tether. For example, considering the LTA4H binding mode of **4**, we reasoned that amendment of **20** with the optimized (*R*)-prolinol linker of DG-051 would yield a more potent molecule, **14** (Scheme 1). Further, on the basis of the structural data for **7**, wherein its aminothiazole was found to displace structurally conserved water molecules deep within the LTA4H active site cavity, we amended **23** to introduce both thiophene and (*R*)-prolinol groups to afford **18** (Scheme 1). Synthesis of the prolinol derived analogue **14** was accomplished by the nucleophilic displacement of tosyl group in **24** with the phenolate derived from 4-benzylaminophenol **20** (Scheme 1). This step was followed by the removal of Boc-protecting group from **25**. The tosylate **24** was prepared following the literature procedure from (*R*)-Boc-prolinol. The Friedel−Crafts acylation of anisole with 4-iodobenzoyl chloride followed by reaction of the methyl ether **22** with boron tribromide in CH_2Cl_2 provided the phenol **23**. The

Scheme 1. Synthetic Routes for New Molecules Inspired by the LTA4H Binding Modes of Compounds **4**, **6**, and **7**[a]

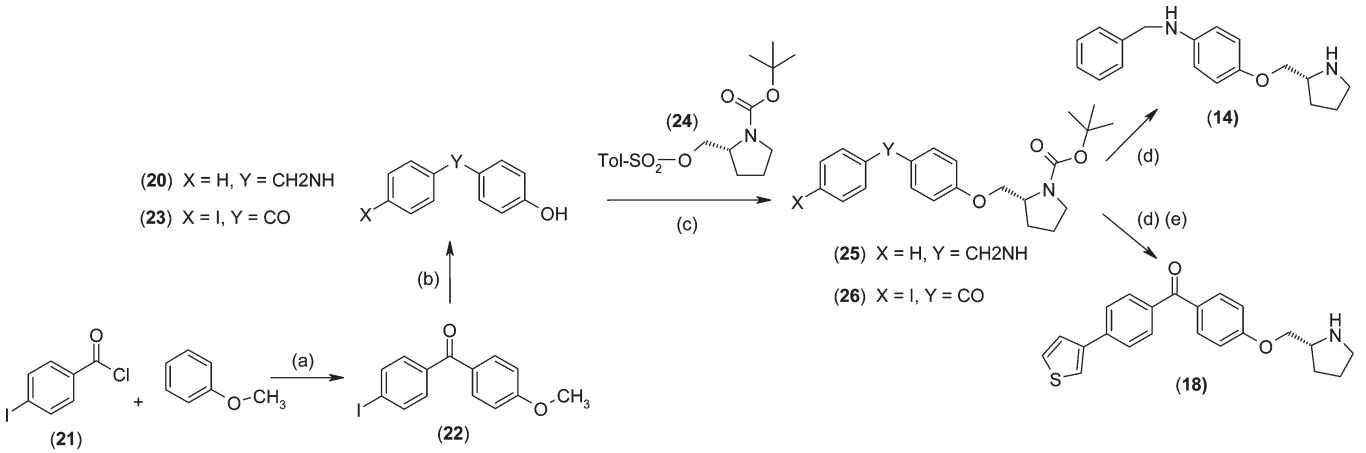

[a] Reagents and conditions: (a) $AlCl_3$, 10 °C, nitrobenzene, 90%; (b), BBr_3, CH_2Cl_2, −78 °C → 0 °C, 85%; (c) NaH/DMF, 0 °C → rt → 90 °C; (d) 1 M HCl/Et_2O, 80−97%; (e) thiophene-3-boronic acid (2 equiv), $Pd(OAc)_2$ (25 mol %), K_2CO_3/EtOH/DME, 90 °C, 60%.

Scheme 2. Elaboration of Fragment **6**[a]

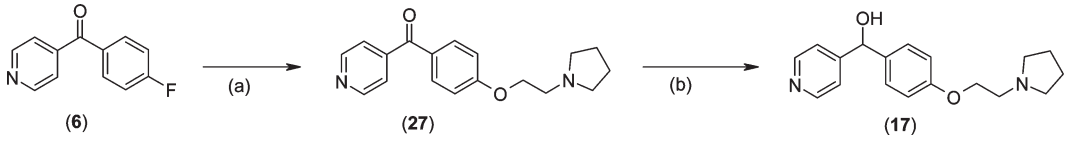

[a] Reagents and conditions used are as follows: (a) 1-(2-hydroxyethyl)pyrrolidine, K-O^{t}Bu, DMSO, 90 °C, 16 h, 54%; (b) $NaBH_4$, MeOH, 40 °C, 4 h.

Scheme 3. Elaboration of Fragment **11**[a]

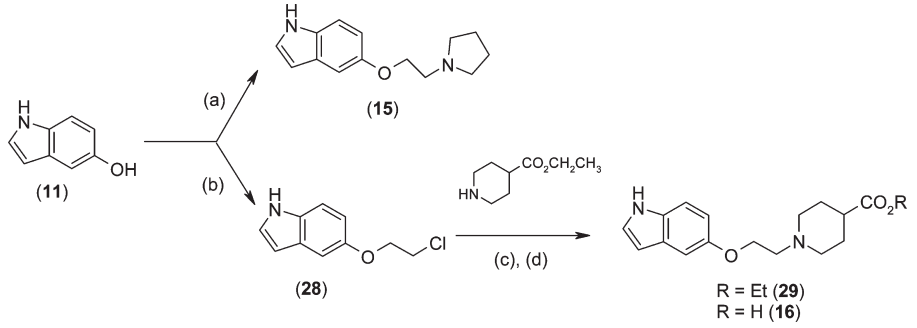

[a] Reagents and conditions: (a) 1-(2-chloroethyl)pyrrolidine, K_2CO_3, acetone, 19%; (b) 1-bromo-2-chloroethane, K_2CO_3, 2-butanone, reflux 60 h, 17%; (c) piperidine-4-carboxylic acid ethyl ester, HCl (2 equiv), KI (0.3 equiv), K_2CO_3, DMF, rt → 90 °C, 57%; (d) aq NaOH, EtOH, rt.

sodium phenolate of **23**, generated in situ with NaH in DMF, was subsequently reacted with the tosylate **24** to provide the BOC protected 4-iodobenzophenone derivative **26**. Stille coupling of **26** with thiophene-3-boronic acid followed by deprotection of the *N*-BOC under acidic conditions provided the compound **18** (Scheme 1).

Subsequent structural studies of **14** revealed that the pyrrolidine moiety was bound at the bend in the LTA4H substrate binding cavity (Figure 2N). It provided the necessary kink for the molecule pivoting toward catalytic Zn^{2+}. Its binding mode resembled the pyrrolidine group orientation in the DG-051-LTA4H complex (Figure 4). It was also similar to the positioning of the phenyl ring of bestatin bound to LTA4H. This allowed the lone electron pair of the nitrogen to form a potential 3 Å hydrogen bond with Oε1 of Gln134. This simple structure-guided modification immediately furnished a 4000-fold improvement in affinity of **14** against the enzyme with IC_{50} values of 207 and 157 nM in the peptidase and hydrolase assays, respectively. Superimposing the structure of **14** with the coordinates of the "fragment plus fragment" structure of **4** with acetate showed that there was a 1.9 Å gap between the methyl carbon of acetate and the nearest carbon atom of the pyrrolidine (Figure 4), suggesting that a single carbon atom linkage between the two components would yield a molecule with LTA4H binding similar to that of DG-051 (Figure 2S). Structural studies of **18** (Figure 2R) confirmed that, similar to **7**, the thiophene moiety displaced two water molecules from the bottom of the substrate binding cavity (Figure 5). The biaryl core of **18** was shifted compared to the parent molecule **6**, moving carbonyl oxygens 5.2 Å apart. This motion likely decreased the unfavorable interaction with the backbone carbonyl of Trp311, resulting in a potent inhibitor with IC_{50} values of 80 nM in the peptidase assay and 189 nM in the hydrolase assay.

To further explore elaboration of fragment **6**, we displaced the fluorine atom in **6** with *N*-pyrrolidin-2-ethanol to furnish

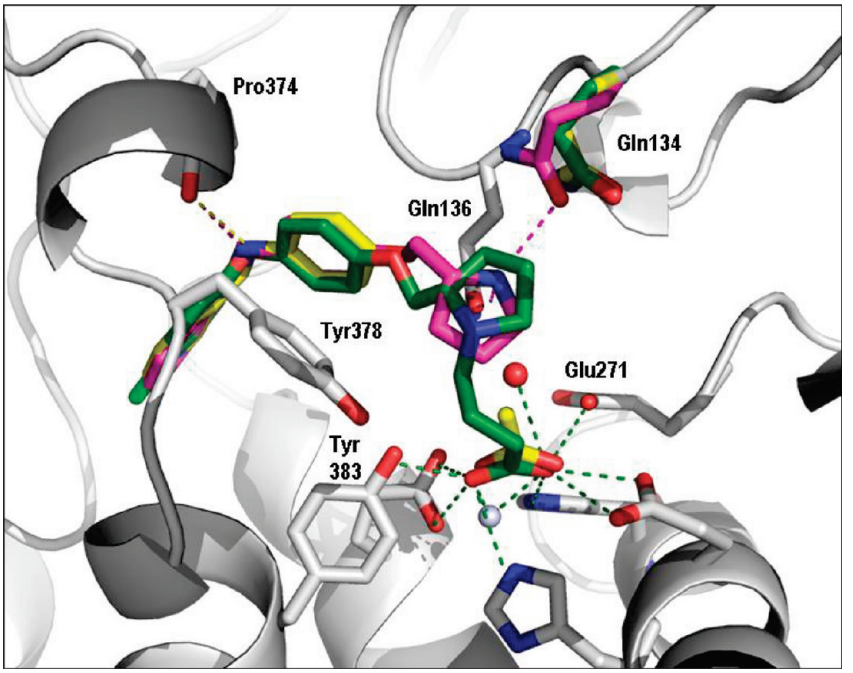

Figure 4. Elaboration of **4**. Refined crystal structures of LTA4H in complex with molecules in the compound **4** elaboration series are shown. Compound **4** and acetate from the "fragment plus fragment" structure are displayed as yellow stick structures, while compound **14** is magenta and compound **19** (DG-051) is green. The side chain conformations of LTA4H bound to each of these compounds are essentially superimposable (gray side chains) with the exception of Gln134, which demonstrates some flexibility in its conformation as represented by DG-051 (green), compound **4** and acetate (yellow), and compound **14** (magenta). Polar contacts are displayed as color-coded dashed lines.

the biaryl ketone **27** (Scheme 2). This intermediate was reduced with sodium borohydride to afford the targeted biaryl carbinol derivative **17** (Scheme 2).

The LTA4H cocrystal structure of **17** revealed a potential hydrogen bond between the OH group in the molecule and the carbonyl of Trp311 (Figure 2Q). Molecule **17** featured an IC_{50} of 202 μM (peptidase assay) and 170 μM (hydrolase assay), which was a 25- to 30-fold improvement over the initial hit **6** but was an order of magnitude less potent than molecule **18**, the more fully elaborated derivative of fragment **6**. This comparison suggests that the improved potency of compound **18** likely results from a combination of water molecule displacement deep within the LTA4H active site pocket by the thiophene, plus the effects of hydrogen bonding between Gln134 and the pyrrolidine of **18**.

Encouraged by these data, we routinely used pyrrolidine-containing moieties in our optimization effort. For example, the 5-hydroxyindole fragment identified earlier as hit **11** was modified with 1-(2-methoxyethyl)pyrrolidine in the presence of K_2CO_3 in acetone (Scheme 3) to afford compound **15** (IC_{50} of about 321 and 234 μM in the peptidase and hydrolase assays, respectively). Structural data suggested that the pyrrolidine moiety of **15** occupied the same space as observed for **14**, with the ring being in proximity to the side chain of Gln134 (Figure 2O).

Considering both activity data and synthetic feasibility, we attempted to replace the pyrrolidine ring of **15** with a piperidine carboxylic acid moiety to furnish **16** (Scheme 3). For the preparation of compound **16**, 5-hydroxyindole **11** was first reacted with 1-bromo-2-chloroethane to provide the 2-chloroethyl ether **28**. Subsequent displacement of the primary chloro group of **28** with piperidine-4-carboxylic acid ethyl ester in refluxing 2-butanone furnished the ester derivative **29**. This compound was further hydrolyzed with NaOH in EtOH to afford the targeted molecule **16**. Structural elucidation of **16** bound to LTA4H revealed that its carboxylic acid moiety was bound to the active site Zn^{2+} (Figure 2P). However, its potency of IC_{50} of about 1491 and 966 μM in the peptidase and hydrolase assays, respectively, was 4-fold less than that of **15**. Notably, the binding modes for molecules **15** and **16** significantly differed. Positioning of indole group (Figure 6) was driven by the orientation of pyrrolidine (for **15**) and piperidine-4-carboxylic acid (for **16**) pharmacophores in the active site of LTA4H.

Discussion

In this work we have combined the concepts of metabolomics with fragment based drug discovery to assemble a ~1300-member "fragments of life" (FOL) small molecule library for screening by X-ray crystallography. This set includes highly soluble metabolites, natural products, their derivatives, and biaryl molecules mimicking architectural motifs found in proteins. Small molecules of life have coevolved with their respective macromolecular targets, and therefore, such interactions are likely to be highly ligand efficient. In addition, signaling pathways are known to display allosteric feedback mechanisms involving small molecules (for a recent review, see Goodey and Benkovic[84]). Consequently, application of molecules of life in the FBDD approach may lead to the identification of novel allosteric binding sites in protein targets. In addition, many molecules of life are likely to feature druglike properties, since these compounds display properties necessary for intracellular activity (e.g., reasonable target affinity, reversible binding, controlled on/off rates, solubility, permeability, etc.).

The FOL library has been designed without target bias. In the initial validation, we screened approximately 200 molecules (15%) of the entire selection (1329 compounds) against LTA4H using X-ray crystallography. Thirteen unique

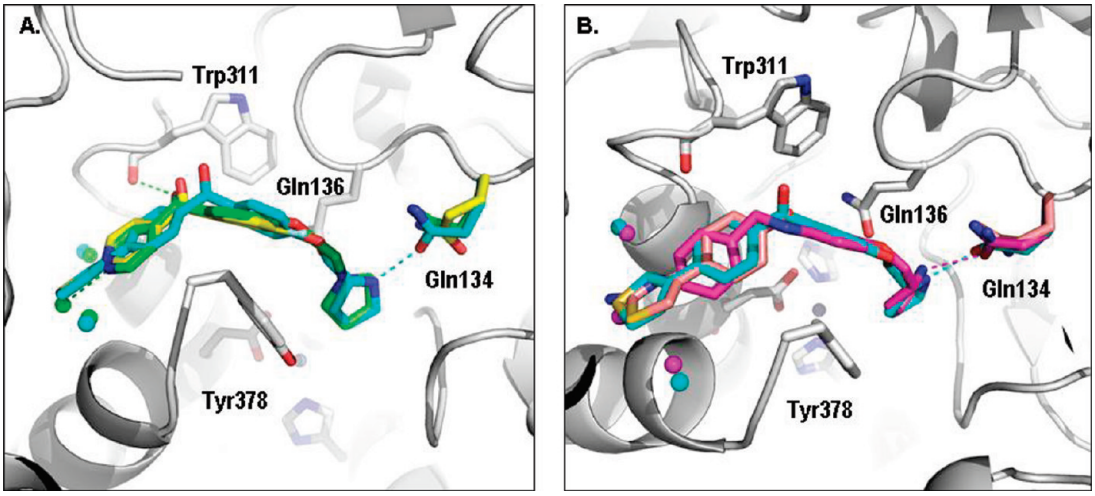

Figure 5. Elaboration of 6. (A) Superposition of compounds **6** (yellow), **17** (green), and **18** (cyan). Invariant portions of the LTA4H structure are colored gray, and compound-specific polar contacts, side chain conformations, and bound water molecules are color-coded by compound. (B) Superpostion of **18** (cyan) with the thiazole-containing fragment **7** (rose) and the pyrrolidine containing compound **14** (magenta). Both **7** and **18** displace the central structurally conserved water molecule, and both **14** and **18** have pyrrolidine moieties that occupy nearly the same space in the LTA4H structures.

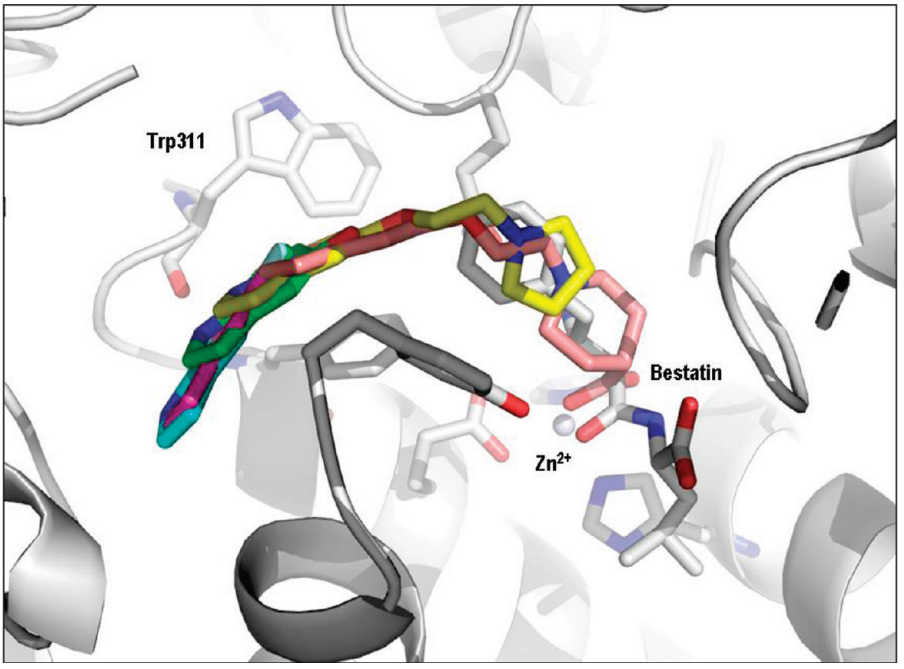

Figure 6. Elaboration of 5-hydroxyindole **11**, showing superposition of the indole-containing fragment structures: 5-hydroxyindole **11** (dark green), 5-chlororindole **12** (magenta), 5-fluoroindole **13** (cyan), and derivative compounds **15** (yellow) and **16** (pink).

fragments were discovered, representing a hit rate of 6%. Most of the identified fragments (12 out of 13) were bound to the active site pocket, while fragment **10** bound within a shallow surface pocket. Fragment **7** interacted with both the active site pocket and the surface of LTA4H. It is noteworthy that the two fragments found binding to the surface of LTA4H were biaryl structures with either a thiophene or thiazole moiety plus at least one amino or hydroxyl group. A similar observation has been reported recently for thiazole derivatives binding at sites of protein−protein interaction,[76] suggesting the possibility that these themes may be exploited to develop specialized fragment libraries to screen for modulators of protein−protein interactions. Importantly, FOL hits varied both structurally and in their source within the library. Specifically, biological molecules FOL-Nat (e.g., resveratrol, dihydroresveratrol, 5-hydroxindole), their derivatives FOL-NatD (e.g., 5-hydroxyindole, nicotinamide, and isonicotinic acid derivatives), and FOL-Biaryls which mimic a protein structure (e.g., fragment **10**) were found to bind to LTA4H in a diverse array of binding modes.

The structures of LTA4H with bound resveratrol (compound **2**) and its metabolite dihydroresveratrol[64,71,72] **3** were of particular interest because of the potential therapeutic implications. As LTA4H is involved in both increased risk of myocardial infarction[29] and inflammation,[30] one may consider attributing the apparent cardioprotective properties of resveratrol and other sirtuin activators[85−87] to LTA4H modulation. Our finding suggests that the FOL approach may

facilitate rational identification of small molecule agents that simultaneously modulate several therapeutically relevant pathways.[8]

The binding of dihydroresveratrol **3** also illustrates the potential utility of "fragment plus fragment" mode of screening. For example, when **3** bound to LTA4H together with bestatin, several structural water molecules were displaced within the LTA4H active site pocket and Phe362 was found to adopt an alternative side chain rotamer conformation. This finding shows that when fragment cocktails are repooled with other fragments, new induced-fit fragment binding modes can be observed.

Using structural guidance from FOL screening, we showed that fragment hits could be expeditiously modified to generate potent LTA4H inhibitors in a short synthetic sequence. The diverse chemical nature of the initial hits suggests that this strategy is applicable to the identification of novel and structurally distinct chemotypes. In a representative example, structural information from diverse active fragments was combined to evolve a fragment hit **6** of very poor activity (IC_{50} = 5.3 mM) in the peptidase assay into a potent LTA4H inhibitor **18** (IC_{50} = 80 nM) in two synthetic steps. Fragment hit **4** was derivatized in a single step to afford **14**, a novel and potent inhibitor of LTA4H (IC_{50} = 150 nM in the hydrolase assay) with comparable potency (IC_{50} = 131 nM) for inhibition of LTB4 production in human whole blood. Compound **14** featured high ligand efficiency of 0.44 kcal/(mol·heavy atom) vs 0.36 kcal/(mol·heavy atom) for the clinical candidate DG-051 **19**. Thus, a combination of properly selected fragments with structural insight into their mode of binding allowed for maintenance of ligand efficiency and druglike potential of the optimized hits.

The FOL library was of value in expanding the known chemical space of LTA4H inhibitors. Our structural studies have consistently identified multiple fragments that exemplify reported LTA4H binders. For example, the binding modes of our compounds **4** and **5** were all superimposed and mimicked the benzoxyphenyl components of LTA4H inhibitors reported by Kirkland et al. (see Supporting Information Figure 4).[40] Furthermore, our ligand docking studies suggest that the predicted binding modes of the LTA4H inhibitors reported by Grice et al. and Rao et al.[39,88] could be emulated with FOL compounds identified in this study. Namely, the indole core of fragments **12** and **13** overlaps well with the benzoxazole or benzothiazole templates described by these authors (see Supporting Information Figure 7). The fluorophenyl ring of **6**, the phenol substituent of **2** and **3**, the phenyl ring of **4**, and **5** all superimpose to emulate the binding mode of the phenoxy pharmacophore featured in the inhibitors reported by Grice et al. and Kirkland et al. (see Supporting Information Figure 8).

Given the importance of LTA4H activity in myocardial infarction[28,29] and inflammatory respiratory disease,[88] we previously reported the development of DG-051 (**19**, Figure 2S). This molecule is a potent inhibitor of LTB4 production in human whole blood (IC_{50} = 37 nM). DG-051 was designed via structure-guided medicinal chemistry. It has recently completed phase IIa clinical trials.[43] The agent comprises three functional components: a butanoic acid, a pyrrolidine linker, and a lipophilic biphenyl ether moiety. As suggested by our structural studies, these pharmacophores were effectively captured with FOL hits. Reversible binding of the butanoic acid moiety of DG-051 to Zn^{2+} in the active site of LTA4H was mimicked by the acetate ion in our "fragment plus fragment" approach (Figure 4). The pyrrolidine linker that provides flexibility for DG-051 to navigate the bend in the substrate binding cavity was largely typified by the prolinol derivatives **14** and **18** as well as the pyrrolidine derivatives **15** and **17**. The biphenyl ether functionality of our clinical candidate binds within the most hydrophobic part of the cleft lined with aromatic amino acid residues including Tyr267, Trp311, and Phe314. Its chlorine substituent resides within ~3.2 Å from one of the three structurally conserved water molecules (in the proximity of Lys364 and Leu365) at the bottom of the L-shaped active site cavity.[43] These binding features of DG-051 were represented by fragments **2**−**9**.

In summary, we introduced a concept of fragments of life (FOL) library for structure-based drug discovery. In proof-of-concept studies, we screened the FOL set against LTA4H by X-ray crystallography. The resulting structural information yielded insight into a novel series of LTA4H binders. It also captured binding trajectories for multiple reported inhibitors of the enzyme. We further demonstrated that the identified fragments could be optimized in a short reaction sequence to yield molecules with high ligand efficiency and potent biological activity. The fragments and their derivatives feature binding efficiency for LTA4H and surface efficiency indices that match those of marketed drugs[16] (see Supporting Information Figure 9). Further studies are required to determine the versatility of the FOL library screening against diverse target classes. It is likely that further chemical amendments to this selection will be needed to enhance hit rates. In addition, the versatility of the FOL set is being tested in different readout platforms including NMR and surface plasmon resonance.

Materials and Methods

Purification of LTA4H. Recombinant human LTA4H (residues 1−611) was expressed in *E. coli* BL21-AI/pRARE. An amount of 7.5 g of cell paste was lysed by nitrogen cavitation at 2200 psi for 1 h in a lysis buffer consisting of 50 mM Tris-HCl, pH 8.0, 1 mM PMSF, 0.2 mg/mL lysozyme, and 1.5 U/mL benzonase. The lysate was clarified by centrifugation at 42 000 rpm for 45 min at 4 °C. Clarified lysate was filtered using a 0.2 μM syringe-top filter. Lysate was then applied to 2 × 5 mM HisTrap HP columns (GE Healthcare) equilibrated with 20 mM Tris-HCl, pH 8.0, and 200 mM NaCl. The column was washed with six column volumes of 30 mM imidazole and eluted with a linear gradient of 30−300 mM imidazole in 20 mM Tris-HCl, pH 8.0, containing 200 mM NaCl. The pooled peak fractions were >95% pure by SDS−PAGE at a concentration of 2.7 mg/mL and used directly for crystallization without further concentration or dialysis.

Crystallization and Fragment Screening. LTA4H was crystallized by sitting drop vapor diffusion against a crystallant containing 100 mM imidazole, pH 6.5, 12.67% w/v PEG-8000, 100 mM sodium acetate, and 5 mM $YbCl_3$. Crystal growth was accelerated through the use of a microseeding protocol. Seed stocks were prepared by suspending several crystals in 20 μL of crystallant and crushing them by vortexing in a Seed Bead tube (Hampton Research). Crushed crystals were diluted 1:100 into fresh crystallant and vortexed again to form the final seed stock. Crystallization drops were set up in a Compact Jr. 96-well crystallization plate (Emerald BioSystems) by combining 0.7 μL of LTA4H (2.7 mg/mL) with 0.7 μL of crystallant and 0.2 μL of seed stock over a reservoir volume of 100 μL.

X-ray Crystallography. Twenty-five pools of eight compounds from the FOL library were screened against LTA4H by X-ray crystallography. Pool stocks consisted of cocktails of eight fragments, each at 6.25 mM in methanol. Individual FOL compounds are stored in barcode labeled sealed septum vials as

50 mM stocks in pure methanol and stored at −20 °C. Approximately 30% of the fragment stocks have been analyzed over a period of 12 months by mass spectrometry to demonstrate general stability of the compounds in methanol (data not shown). Fragment cocktails in methanol were spotted onto the drop chambers of crystallization plates and the solvent was allowed to evaporate, leaving a precise amount of fragment compounds as a dry powder with no solvent residue that could potentially interfere with crystallization or crystal stability. A volume of crystallization mother liquor equal to the initial volume of fragment cocktail was added to the dry powder, allowing for dissolution of the fragments. Crystals were transferred to the resulting solution and allowed to soak overnight. This technique is versatile, as it is suitable for both cocrystallization and soaking experiments, and adjusting ratios of methanol solution to crystallant solution allows for adjustment of the final fragment concentration in the drop.

Although diversity pooling was conducted to aid in identification of fragments from pool density alone, factors such as low resolution, low occupancy, or competitive binding can lead to uncertainty. Therefore, in cases where crystals exposed to fragment cocktails produce difference electron density indicative of fragment binding, follow-up experiments with individual fragments were performed. During this deconvolution step, individual candidate fragments were soaked into crystals, usually at 10−25 mM. The resulting crystal structures provide unambiguous confirmation of fragment hits, and all structures presented were generated from single molecule crystal soaking experiments.

LTA4H Peptidase Activity Assay. L-Arginine-*p*-nitroanilide (Arg-*p*NA) substrate was obtained from Sigma. Stock solution of ARG-*p*NA (500 mM) was prepared and serially diluted in DMSO. Final peptidase assays were performed in 96-well clear, flat bottom plates (Corning). Each assay plate contained eight positive (no inhibitor) and eight negative (no enzyme) controls. LTA4H (45 μL) and test compounds (5 μL) were preincubated for 10 min followed by addition of substrate (50 μL); final reactions contained 100 mM Tris-HCl (pH 8.0), 100 mM NaCl, 5% DMSO, 0.5 mM Arg-*p*NA, and 20 nM LTA4H. Control experiments showed that 5% DMSO had no effect by itself on enzyme activity (data not shown). Reaction rates were monitored in a SpectraMax 190 plate reader (Molecular Devices) at room temperature (rt) by measuring the increase in absorbance at 410 nm due to cleavage of the amide bond of the substrate and formation of *p*-nitroaniline. Reactions were measured for 30 min, and initial rates were determined from the linear portions of the progression curves using SoftMax Pro software (Molecular Devices). Dose−response curves ware calculated by fitting data to a sigmoidal four-parameter logistic equation using Prism (Graphpad).

LTA4H Hydrolase Activity Assay. LTA_4 substrate was prepared from the methyl ester of LTA_4 (BioMol or Cayman Chemicals) by treatment under nitrogen with 100 mol equiv of NaOH in an acetone/H_2O (4:1) solution at rt for 40 min. Stock solutions of LTA_4 were kept frozen at −80 °C for a maximum of 1 week prior to use. Recombinant human LTA_4H (10 nM final concentration) was incubated with various concentrations of test compound for 10 min at rt in assay buffer (0.1 M Tris-HCl, 0.1 M NaCl, 5 mg/mL fatty acid free BSA, 10% DMSO, pH 8.0). Immediately before the assay, LTA_4 was diluted in assay buffer (without DMSO) and added to the reaction mixture to a final concentration of 1 μM to initiate the enzyme reaction. Samples were incubated for 10 min at rt followed by addition of 2 volumes of chilled quenching buffer (CH_3CN with 1% CH_3COOH and 73 nM LTB_4-d_4 (BioMol). The samples were then stored at 4 °C for 12 h to complete protein precipitation and centrifuged for 15 min at 1800*g*. LTB_4 formed was measured in the supernatant by LCMS/MS using LTB_4-d_4 as an internal standard and an external LTB_4 standard (BioMol) for a calibration curve. Briefly, the analyte was separated from LTB_4 isomers formed by spontaneous hydrolysis of LTA_4 using isocratic elution on an HPLC system (Waters) and analyzed on a tandem quadrupole mass spectrometer (Waters Micromass Quattro Premier). MRM transitions followed on two channels were 335.2 → 195.3 (LTB_4) and 339.2 → 197.3 (LTB_4-d_4). On the basis of the measured amounts of LTB_4 formed at each inhibitor concentration, a dose−response curve was fitted to the data using a sigmoidal four-parameter function (Prism, Graphpad) and an IC_{50} value was calculated. Ligand efficiency values were calculated for hydrolase and peptidase assays independently using LE (kcal/(mol·HA)) = $-RT\ln(IC_{50})/HA = -0.59179(\ln IC_{50})/HA$, where HA is the number of heavy atoms (nonhydrogen).

Human Whole Blood LTB_4 Assay. Human blood (45 mL) was collected in heparin-containing Vacutainer tubes (Greiner-Bio One) with informed consent. Individual experiments were performed with blood from a single subject. For each sample, 200 μL of blood was dispensed into a prewarmed 96-well plate and 188 μL of RPMI-1640 medium (Invitrogen) containing 20 μg/mL indomethacin (Sigma) was added. An amount of 4 μL of a series of compound dilutions (final DMSO concentration of 1%) was added in triplicate, followed by a 15 min incubation at 37 °C with gentle shaking. Blood samples were stimulated by adding 8 μL of ionomycin (from *Streptomyces conglobatus*, Calbiochem) to a final concentration of 36 μM. After another incubation at 37 °C for 30 min, samples were centrifuged at 4 °C for 5 min at 1800*g*. LTB_4 concentrations in supernatants were determined using a commercially available enzyme-linked immunosorbent assay (R&D Systems) according to the manufacturer's instructions. On the basis of the measured amounts of LTB_4 formed at each inhibitor concentration, a dose−response curve was fitted to the data using a sigmoidal three-parameter function (XLfit, IDBS), and an IC_{50} value was calculated. Each assay plate contained eight positive controls (no compound) and eight negative controls (no Ionomycin).

Fragment Selection for the Fragments of Life Library. Approximately 400 candidate fragments representing natural molecules of life with (i) molecular weights less than 350, (ii) fewer than six hydrogen bond donors, and (iii) fewer than seven hydrogen bond acceptors were manually selected from known metabolic pathways. Molecules were selected from eukaryotic, archaebacterial, and eubacterial metabolic pathways and from presumed primordial pathways.[89,90] There was no bias toward any particular metabolic pathway; however, molecules of conserved intermediary metabolism were prioritized.[91] Approximately 300 of the resulting fragments were commercially available, reasonably priced, and acquired. These fragments were tested for solubility (≥50 mM in methanol) to yield a final core set of 218 natural molecules (FOL-Nat). The chemical diversity of the first 218 FOL-Nat fragments was determined using a 210 × 210 principal component analysis (PCA) using Cerius^2 (Accelrys). In this analysis 1D, 2D, and 3D descriptors (conformational, cat shape, electronic, quantum chemical, information content, spatial, structural, thermodynamical, topological, and geometrical) were calculated and the 3D distribution of the fragments was visualized in a 3D plot (see Supporting Information Figure 2). This analysis showed that the fragments were diverse but did not densely cover the desired chemical space. Therefore, in addition to the manual selection, we explored the Available Chemicals Directory (ACD/Lab, version 7, MDL) and the Maybridge Fragment Library (www.maybridge.com) as a source of additional fragments. We intended to diversify the original set by selecting heteroatom-containing derivatives of natural molecules (FOL-NatD) with fragment-like properties. Toward this goal, a selection of 238 996 compounds were analyzed using modified "rule of three"[11] parameters to afford 49 877 fragments with (i) molecular weights between 110 and 250 Da, (ii) calculated log of octanol/water partition coefficient (ClogP) of less than or equal to 3.0 (calculated with software available from Daylight

Chemical Information Systems, Inc.), (iii) hydrogen bond donors less than or equal to 3, and (iv) hydrogen bond acceptors less than or equal to 6 (calculated with Sybyl, version 6.8, Tripos). Virtual selection of the 49 877 molecules was further subjected to a panel of SMARTS filters[92] in order to eliminate molecules endowed with problematic functionalities. A partial list of these SMARTS filters included reactive functional groups, lipophilic chains of seven or more carbon atoms, crown ethers, disulfides, excessive (> 3) acidic groups, thiols, epoxides, aziridines, hydrazones, thioureas, thiocyanates, benzylic quaternary nitrogens, thioesters cyanamide, four membered lactones, di- and triphosphates, metals, phosphines, phosphonic acids, sulfonic acids, sulfonyl halides, boronic acids, isotopes, salts, metals, more than 3 halogens, more than two nitro groups, and lanthanides. This culling process resulted in 40 489 candidate fragment compounds. Each fragment from the resultant filtering was converted from 2D to 3D projection using CONCORD (Tripos) and used to identify fragments with ≤3 rotatable bonds and calculated PSA values of ≤60 Å^2. The resulting 5606 fragments were again analyzed using the previously described principal component analysis (PCA), and 1016 unique fragments were selected with preference for molecules that could be visually identified to have at least 8 atoms with chemical arrangements that matched that of a known natural molecule of life. From this set, 880 fragments were commercially available and obtained at a reasonable price. These fragments were tested for solubility (> 50 mM in methanol), and the resulting 666 fragments (FOL-NatD) were added to the FOL library. PCA analysis showed that the FOL-NatD fragments occupy distinctly different chemical space (see Supporting Information Figure 2) and that together the FOL-Nat and Fol-NatD fragments combine to form a diverse and relatively dense set of fragments. Finally, we were also intrigued by the possibility of mimicking a protein 3D architecture using biaryl small molecule fragments.[59−61,93] In order to identify protein mimetic fragments (FOL-Biaryl), we first identified 566 molecules containing 5−5, 6−5, and 6−6 biaryls connected via a σ-bond to allow for a controlled torsional freedom from the ChemBlock library (www.chemblock.com). The energy minimized conformations (Tripos force field, Sybyl 6.8) of a selection of these biaryl fragments were overlaid with the α, β, γ turns of a known protein structure (1RTP.pdb) and shown to have good steric and electronic mimicry of protein structure. The resulting fragments were tested for solubility (> 50 mM in methanol), resulting in 445 fragment molecules (FOL-Biaryl). Results from the PCA analysis and physical properties of the fragments [MW, ClogP, total polar surface area, number of hydrogen bond donor/acceptors, rotatable bonds, and rings] of the complete 1329 member FOL library are provided in Supporting Information (see Supporting Information Figure 1).

Computational and Physical Pooling. When fragments are pooled into structurally diverse cocktails of 4−10 compounds per mix, the throughput of X-ray screening of fragment libraries can be significantly increased.[12,94,95] The pooling of fragments was carried out using the same 210 × 210 descriptor space principle component analysis (Cerius^2, Accelrys) in order to select eight diverse fragments per pool. The nature of the fragment (FOL-Nat, FOL-NatD, FOL-Biaryl) was not considered in the pooling strategy. Monte Carlo optimization using "Diversity Metric Function MAXMIN Distance" (Accelrys) with the optimum distance range of 1.97−2.57 Å was used to randomly extract eight diverse fragments. After extraction of eight fragments from the library, the process was repeated until the entire library was computationally pooled into structurally diverse pools each containing eight fragments. Individual fragments, each >95% pure as determined by NMR spectroscopy, were prepared as 50 mM stocks in methanol. Physical pools of eight fragments each were prepared by mixing fragment stocks such that the final concentration of each was ∼6 mM. The fragment pools were found to be visibly stable, with no observed precipitation, suggesting that fragment pairs or combinations do not have a propensity to aggregate.

Molecular Docking. The ligand docking into LTA4H was carried out with the Surflex interface implemented in Sybyl 7.2 (Tripos Inc., St. Louis, MO). The Surflex-Dock engine uses an empirical scoring function and a patented search engine to dock ligands into a protein's binding site.[96] The PDB ID 3CHI file was converted to a mole2 file, and hydrogens were added. The *B*-values were replaced by the AMBER charges using Sybyl 7.2. The bound ligand of 3CHI was removed from the binding site. The Surflex-Dock protomol, a computational representation of the intended binding site, was generated using the probes CH_4, −N−H, and −C═O. The protomol directed the placement of the ligand during the docking process. LTA4H inhibitors were drawn in ISIS Draw and converted to 3D structures with CONCORD of Sybyl 7.2 (Tripos Inc., St. Louis, MO). All of the inhibitors were properly typed with hydrogens, and a 3D structure data file was created for docking. Each ligand was then fragmented which reduced the conformational space to be explored. The fragments were then aligned to the protomol probes. All the fragments were scored,[97] and the highest scoring fragment was kept as the head fragment. The tail fragments were selected on the basis of the similar principle, and gradual attachment was carried out to build the docked ligand. The poses were refined, eliminating those with excessive penetration into the protein. Thirty poses for each of the ligand were generated and visualized in the active site based on their Surflex scores. The best fitting ligand poses were chosen for further comparative structural analysis.

General Methods. All reagents and anhydrous solvents were obtained from commercial sources and used without further purification unless otherwise noted. NMR spectra were recorded at 400 or 500 MHz (Varian Instruments) in the solvent indicated, and TMS was used as an internal reference. ACDLabs NMR software was used to process FIDs to generate spectral parameters (δ (ppm)/Hz). Coupling constants (*J*) are given in Hz. Mass spectra were obtained using either APCI or electrospray ionization (PE-SCIEX single-quad or Agilent mixed-mode units). Elemental analyses were carried out by Galbraith Laboratories, Inc. (Knoxville, TN) or Midwest Microlab, LLC (Indianapolis, IN). Column chromatography was carried out in the solvents indicated with silica gel (MP EcoChrom, 32-63D, 60 Å). The HPLC method was as follows. Compounds were eluted using a gradient of 90/10 to 10/90 A/B over 40 min at a flow rate of 1.0 mL/min, where solvent A was 0.05% TFA in 100% H_2O and solvent B was 0.05% TFA in 100% acetonitrile. For HPLC data (final products), peak area percent and retention time (t_R in min) are provided. The following compounds were obtained from commercial sources: compound **4** from Matrix, compounds **5**, **7**, **8**, **9**, and **10** from Maybridge, compound **6** from VWR, and compounds **11**, **12**, and **13** from Aldrich.

Benzyl[4-((*R*)-1-pyrrolidin-2-ylmethoxy)phenyl]amine (14). To a solution of **25** (148 mg, 0.387 mmol) in methanol (3 mL) was added HCl (1 M in diethyl ether, 6 mL). The mixture was stirred at rt for 3 h. The solvent was removed in vacuo to provide the title compound **14** as a hydrochloride salt (128 mg, 93%). ^{1}H NMR (400 MHz, DMSO-d_6) δ 1.60−1.73 (m, 1H), 1.87−2.12 (m, 3H), 3.17−3.21 (m, 2H), 3.84−3.87 (m, 2H), 4.19−4.23 (dd, 1H J_1 = 3.6 Hz, J_2 = 10.8 Hz), 4.11−4.16 (m, 1H), 4.44 (s, 2H), 7.0 (d, 2H J = 8.8 Hz), 7.29−7.38 (m, 5H), 7.48−7.49 (m, 2H) 9.1 (s, 1H), 9.8 (s, 1H). LCMS: 97%; APCI$^+$ m/z 283 (M + 1). Anal. ($C_{18}H_{22}N_2O \cdot 2HCl$) C, H, N.

5-(2-Pyrrolidin-1-ylethoxy)-1*H*-indole (15). To a solution of 5-hydroxyindole **11** (446 mg, 3.35 mmol) in anhydrous acetone (20 mL) was added potassium carbonate (1.36 g, 9.8 mmol) and 1-(2-chloroethyl)pyrrolidine hydrochloride (1.28 g, 7.5 mmol). The reaction was heated to reflux for 16 h. After the mixture was cooled to rt, a solution of tetrabutylammonium bromide (200 mg, 0.6 mmol) in DMF (10 mL) was added and the mixture

was heated to 55 °C for 16 h. The solvent was removed in vacuo, and the resulting residue was partitioned between EtOAc (25 mL) and water (50 mL). The organic layer was separated, dried with anhydrous $MgSO_4$, and concentrated in vacuo to an oil. The oil was purified by silica gel flash chromatography (~100 g of SiO_2, 0−5% MeOH/CH_2Cl_2, gradient) to provide the title compound **15** (145 mg, 19%). ^{1}H NMR (400 MHz, DMSO-d_6) δ 1.68 (dt, J = 6.57, 3.15 Hz, 4 H), 2.53 (br s, 4 H), 2.78 (t, J = 6.04 Hz, 2 H), 4.03 (t, J = 6.04 Hz, 2 H), 6.31 (br s, 1 H), 6.71 (dd, J = 8.72, 2.42 Hz, 1 H), 7.03 (d, J = 2.15 Hz, 1 H), 7.23−7.29 (m, 2 H), 10.88 (br s, 1 H). LCMS (APCI$^+$): mass calcd for $C_{14}H_{18}N_2O$, 230.3; m/z found 231 (M + 1), 99%. HPLC: 98.9%, t_R = 10.32 min.

1-[2-(1*H*-Indol-5-yloxy)ethyl]piperidine-4-carboxylic Acid (16). To a solution of **29** (145 mg, 0.46 mmol) in 5% EtOH/H_2O (0.1 mL) was added 50% aqueous NaOH (0.07 mL, 1.15 mmol). The mixture was stirred for 16 h at rt. The reaction mixture was concentrated to ~$^1/_2$ volume and neutralized (pH ~7) with 1 M HCl. The solution was washed with 3 × 20 mL of EtOAc. The remaining aqueous layer was concentrated in vacuo to give a crude residue, which was purified by preparatory thin layer chromatography (C-18, 1:2 CH_3CN/H_2O) to provide the title compound **16** (16.7 mg, 13%). LCMS (APCI$^+$): mass calcd for $C_{16}H_{20}N_2O_3$, 288.3; m/z found 289 (M + 1), 99%. ^{1}H NMR (400 MHz, MeOH-d_4) δ 2.07 (br s, 4 H), 2.39 (br s, 1 H), 2.99 (br s, 2 H), 3.40 (t, J = 4.70 Hz, 2 H), 3.48 (d, 2 H), 4.30 (t, J = 5.03 Hz, 2 H), 6.37 (d, J = 2.95 Hz, 1 H), 6.83 (dd, J = 8.72, 2.28 Hz, 1 H), 7.14 (d, J = 2.28 Hz, 1 H), 7.20 (d, J = 2.95 Hz, 1 H), 7.29 (d, J = 8.72 Hz, 1 H). HPLC: 95.9%, t_R = 10.25 min.

Pyridin-4-yl[4-(2-pyrrolidin-1-ylethoxy)phenyl]methanol (17). To a solution of **27** (500 mg, 1.7 mmol) in MeOH (4 mL) was added sodium borohydride (280 mg, 7.4 mmol) portionwise over 5 min. The mixture was stirred at rt for 16 h and then warmed to 40 °C for 4 h. The mixture was concentrated in vacuo, and the resulting residue was partitioned between 50 mL of saturated NH_4Cl (aq) and EtOAc (25 mL). The organic layer was washed with water (25 mL) and brine (25 mL), then dried over Na_2SO_4, and concentrated in vacuo. The crude material was purified by preparatory thin layer chromatography (SiO_2, 10% 7 N NH_3 in MeOH/CH_2Cl_2 (1:20), isocratic) to provide the title compound **17** (18 mg, 4%). LCMS (APCI$^+$): mass calcd for $C_{18}H_{22}N_2O_2$, 298.3; m/z found 299 (M + 1), 99%. ^{1}H NMR (400 MHz, DMSO-d_6) δ 1.67 (t, J = 3.09 Hz, 4 H), 2.76 (t, J = 5.84 Hz, 2 H), 4.02 (t, J = 5.90 Hz, 2 H), 5.65 (d, J = 3.76 Hz, 1 H), 6.00 (d, J = 4.03 Hz, 1 H), 6.87 (d, J = 8.59 Hz, 2 H), 7.26 (d, J = 8.59 Hz, 2 H), 7.34 (d, J = 5.77 Hz, 2 H), 8.47 (d, J = 5.77 Hz, 2 H). HPLC: 97.7%, t_R = 3.19 min.

(*R*)-2-[4-(4-Thiophene-3-ylbenzoyl)phenoxymethyl]pyrrolidine (18). In a pressure resistant vial, a suspension of **26** (250 mg, 0.5 mmol), thiophene-3-boronic acid (130 mg, 1 mmol), palladium-(II) acetate (20 mg, 0.1 mmol), and triphenylphosphine (60 mg, 0.25 mmol) in DME (10 mL) was stirred, and a mixture of K_2CO_3 (500 mg, 3 mmol) in EtOH (1 mL) and water (1 mL) was added at rt. The tube was sealed, and the mixture was allowed to stir at rt for 30 min, and then it was heated to 90 °C for 16 h. The mixture was cooled to rt and poured into ice−water (200 mL). The resulting material was extracted with EtOAc (250 mL). The organic layers were washed with water (100 mL) and brine (100 mL), then dried over anhydrous Na_2SO_4. The solvent was removed in vacuo to obtain the crude product. Purification (~75 g of SiO_2, 0−20% EtOAc/hexanes, gradient) provided the desired product, BOC-protected intermediate (130 mg, 60%), which was used as such for the next step. To this material (50 mg, 0.1 mmol) dissolved in dioxane (2 mL) was added HCl (4 M in dioxane, 2 mL) at 0 °C. The mixture was allowed to warm to rt and was stirred for 16 h. The solvent was reduced to 1 mL, and Et_2O (15 mL) was added to form a precipitate. The resulting solid was filtered and dried in vacuo to provide the title compound **18** as a hydrochloride salt (30 mg, 80%). ^{1}H NMR (400 MHz, DMSO-d_6) δ 1.91−2.31 (m, 4H), 3.26−3.40 (m, 2H), 4.05−4.10 (m, 1H), 4.20−4.25 (m, 1H), 4.46 (dd, 1H, J_1 = 10.8 Hz, J_2 = 3.6 Hz), 7.16 (d, J = 9.2 Hz, 2H), 7.53−7.57 (m, 2H), 7.78−7.87 (m, 7H). LCMS (APCI$^+$): mass calcd for $C_{22}H_{21}NO_2S$, 363.5; m/z found 364.7 (M + 1), 98%.

4-Iodophenyl)(4-methoxyphenyl)methanone (22). Nitrobenzene (45 mL) was cooled in an ice bath and treated portionwise with $AlCl_3$ (13.5 g, 101 mmol, 1.15 equiv) and followed by addition of 4-iodobenzoic acid chloride **21** (25 g, 94 mmol, 1.07 equiv) in nitrobenzene (25 mL) while maintaining a maximum of 10 °C. The reaction mixture was stirred at 0 °C for 10 min, whereupon anisole (9.5 g, 88 mmol, 1 equiv) was added dropwise in such a manner that the temperature didn't exceed 10 °C. The solution was left to warm to rt overnight. The yellow suspension was poured into ice−water (750 mL). The precipitate was collected by filtration and washed with water (3 × 25 mL). Residue was dissolved in CH_2Cl_2 (1 L), washed sequentially with aqueous $NaHCO_3$ (2 × 150 mL), dried over anhydrous $MgSO_4$, and concentrated in vacuo to provide the title product **22** (26.7 g, 90%). ^{1}H NMR (400 MHz, $CDCl_3$) δ 3.89 (s, 3H), 6.96 (d, J = 8.4 Hz, 2H), 7.48 (d, J = 8.0 Hz, 2H), 7.79 (d, J = 8.4 Hz, 2H), 7.84 (d, J = 8.0 Hz, 2H). MS (APCI$^+$): mass calcd for $C_{14}H_{11}IO_2$, 338.2; m/z found 339.3 (M + 1).

(4-Hydroxyphenyl)(4-iodophenyl)methanone (23). To a solution of **22** (1.7 g, 14 mmol) in CH_2Cl_2 (20 mL) was added 1 M BBr_3 in CH_2Cl_2 (15 mL, 15 mmol) at −78 °C. The resulting mixture was allowed to warm to rt and was stirred for 6 h. The mixture was poured onto 50 mL of ice−water and extracted with CH_2Cl_2 (2 × 100 mL). The combined organic layers were washed with water (50 mL) and brine (50 mL) and dried over anhydrous Na_2SO_4. The solvent was removed in vacuo to obtain the crude product which was purified by recrystallization from acetone−EtOAc−hexane (~1:2:1) to provide the desired product **23** as a white solid (1.4 g, 85%). ^{1}H NMR (400 MHz, $CDCl_3$) δ 6.76 (d, J = 8.5 Hz, 2 H), 6.92 (d, J = 8.1 Hz, 2 H), 7.03 (d, J = 8.3 Hz, 2 H), 7.60 (d, J = 8.2 Hz, 2 H).

(*R*)-2-(Toluene-4-sulfonyloxymethyl)pyrrolidine-1-carboxylic Acid *tert*-Butyl Ester (24). To a stirred solution of (*R*)-2-hydroxymethylpyrrolidine-1-carboxylic acid *tert*-butyl ester (12.0 g, 60 mmol) in pyridine (100 mL) at 5 °C is added *p*-toluenesulfonyl chloride (11.6 g, 60 mmol). The mixture is allowed to warm to rt and is stirred for 16 h. The solvent is removed in vacuo, and the resulting residue was partitioned between EtOAc (500 mL) and water (250 mL). The organic layer was washed with brine (2 × 125 mL) and dried over anhydrous Na_2SO_4. The solvent was removed in vacuo to obtain the product **24**, which was used for the next step without further purification (18.9 g, 90%). ^{1}H NMR (400 MHz, $CDCl_3$) δ 1.39 (d, J = 15.3 Hz, 9 H), 1.65 (br s, 2 H), 1.75−1.85 (m, 1 H), 1.87−1.98 (m, 2 H), 2.40 (d, J = 8.9 Hz, 1 H), 2.45 (s, 3 H), 3.30 (m, J = 6.2 Hz, 1 H), 3.81−4.02 (m, 1 H), 4.06−4.12 (m, 1 H), 7.35 (d, J = 4.2 Hz, 2 H), 7.78 (d, J = 8.2 Hz, 2 H).

(*R*)-2-(4-Benzylaminophenoxymethyl)pyrrolidine-1-carboxylic Acid *tert*-Butyl Ester (25). To a solution of 4-benzylaminophenol (200 mg, 1 mmol) in DMF (3 mL) at 0−5 °C was added NaH (60% in mineral oil, 48 mg, 1.2 mmol) at 0−5 °C. The mixture was stirred at rt for 15 min. A solution of **24** (356 mg, 1 mmol) in DMF (2 mL) was added to the above mixture at 0−5 °C. The reaction mixture was warmed to rt and then heated to 90 °C for 15 h. The resulting mixture was concentrated in vacuo and partitioned between 25 mL of saturated $NaHCO_3$ (aq) and 25 mL of EtOAc. The organic layer was separated, dried over anhydrous $MgSO_4$, and concentrated in vacuo to obtain ~400 mg of crude product, which was purified by flash chromatography (~50 g of SiO_2, 12% EtOAc/hexanes, isocratic) to provide the desired product **25** (169 mg, 44%). ^{1}H NMR (400 MHz, $CDCl_3$) δ 1.47 (s, 9 H), 1.78−2.10 (m, 4 H), 3.26−3.47 (m, 2 H), 3.64−3.76 (m, 1 H), 3.76−3.90 (m, 1 H), 3.99−4.18 (m, 2 H), 4.29 (s, 2 H), 6.60 (d, J = 8.7 Hz, 2 H), 6.80 (d, J = 8.1 Hz, 2 H), 7.29−7.41 (m, 5 H).

(*R*)-2-[4-(4-Iodobenzoyl)phenoxymethyl]pyrrolidine-1-carboxylic Acid *tert*-Butyl Ester (26). To a suspension of NaH (60% in mineral oil, 60 mg, 1.5 mmol) in DMF (10 mL) at 0 °C was added

23 (324 mg, 1 mmol). The mixture was allowed to warm to rt and was stirred for 30 min. The mixture was again cooled to 0 °C, and **24** (400 mg, 1.1 mmol) in 1 mL DMF was added. The resulting mixture was allowed to warm to rt, stirred for 30 min, and heated to 95 °C for 16 h. The reaction was cooled to rt and poured into ice−water (100 mL), and the mixture was stirred for 30 min. The resulting solid was filtered and dried in vacuo to provide the desired product **26** (280 mg, 60%). ^{1}H NMR (400 MHz, $CDCl_3$) δ 0.81−0.92 (m, 2 H), 1.27 (s, 2 H), 1.49 (br s, 8 H), 1.56 (s, 7 H), 2.01−2.09 (m, 1 H), 6.96−7.05 (m, 2 H), 7.48 (d, J = 8.2 Hz, 2 H), 7.78 (d, J = 8.7 Hz, 1 H), 7.85 (d, J = 8.1 Hz, 1 H).

Pyridin-4-yl[4-(2-pyrrolidin-1-ylethoxy)phenyl]methanone (27). A solution of (4-fluorophenyl)pyridin-4-yl-methanone **6** (1.5 g, 7.5 mmol) in anhydrous DMSO (45 mL) was cooled to 0 °C, and potassium *tert*-butoxide (1.0 g, 8.9 mmol) and 1-(2-hydroxyethyl)pyrrolidine (0.95 mL, 8.1 mmol) were added. The resulting mixture was warmed to rt and then heated to 90 °C for 16 h. The reaction mixture was poured into ice−water (100 mL) and extracted with 3 × 25 mL of EtOAc. The organic layer was washed with water (50 mL) and brine (50 mL), then dried over anhydrous $MgSO_4$ and concentrated in vacuo. The crude mixture was purified by flash chromatography (~150 g of SiO_2, 0−7.5% 7 N NH_3 in 1:20 MeOH/CH_2Cl_2 mixture, gradient) to provide the title compound **27** (1.2 g, 54%). ^{1}H NMR (400 MHz, MeOH-d_4) δ 1.86 (dt, J = 6.54, 3.24 Hz, 4 H), 2.73 (br s, 4 H), 3.00 (t, J = 5.50 Hz, 2 H), 4.26 (t, J = 5.50 Hz, 2 H), 7.11 (d, J = 8.86 Hz, 2 H), 7.64 (d, J = 5.90 Hz, 2 H), 7.84 (d, J = 8.86 Hz, 2 H), 8.74 (d, J = 6.04 Hz, 2 H). LCMS (ESI$^+$): mass calcd for $C_{18}H_{20}N_2O_2$, 296.4; m/z found 297.7 (M + 1).

5-(2-Chloroethoxy)-1*H*-indole (28). To a solution of 5-hydroxyindole **11** (2.7 g, 20 mmol) in 2-butanone (50 mL) was added potassium carbonate (5.5 g, 40 mmol) and 1-bromo-2-chloroethane (2.0 mL, 24 mmol). The suspension was stirred under argon and heated to reflux for 60 h. The reaction mixture was filtered, and the filtrate was concentrated in vacuo. The resulting residue was purified by flash chromatography (~200 g of SiO_2, CH_2Cl_2/hexanes, 1:2) to provide **28** (650 mg, 17%). ^{1}H NMR (400 MHz, $CDCl_3$) δ 3.84 (t, J = 6.0 Hz, 2 H), 4.29 (t, J = 6.0 Hz, 2 H), 6.50 (br s, 1 H), 6.91 (dd, J = 8.8, 2.3 Hz, 1 H), 7.15 (d, J = 2.1 Hz, 1 H), 7.21 (t, J = 2.7 Hz, 1 H), 7.31 (d, J = 8.9 Hz, 1 H).

1-[2-(1*H*-Indol-5-yloxy)ethyl]piperidiine-4-carboxylic Acid Ethyl Ester (29). To a stirred mixture of **28** (150 mg, 0.75 mmol), potassium carbonate (207 mg, 1.5 mmol), and potassium iodide (46 mg, 0.28 mmol) in DMF (6 mL) was added piperidine-4-carboxylic acid ethyl ester (0.23 mL, 1.5 mmol). The reaction mixture was heated to 90 °C for 16 h. After cooling to rt, the mixture was diluted with water (6 mL) and stirred for 2 h. The supernatant liquid was decanted from the resulting residue, which was purified by flash chromatography (~25 g of SiO_2, 0−3% MeOH/CH_2Cl_2, gradient) to provide **29** (145 mg, 57%). ^{1}H NMR (400 MHz, $CDCl_3$) δ 1.26 (t, J = 7.2 Hz, 3 H), 1.75−1.88 (m, 2 H), 1.89−1.97 (m, 2 H), 2.15−2.25 (m, 2 H), 2.25−2.36 (m, 1 H), 2.83 (t, J = 6.0 Hz, 2 H), 3.01 (d, J = 11.7 Hz, 2 H), 4.10−4.20 (m, 4 H), 6.48 (br s, 1 H), 6.88 (dd, J = 8.8, 2.3 Hz, 1 H), 7.12 (d, J = 2.0 Hz, 1 H), 7.19 (t, J = 2.7 Hz, 1 H), 7.30 (d, J = 1.0 Hz, 1 H), 8.07 (br. s, 1 H).

Acknowledgment. The authors gratefully acknowledge the contributions of current and former members of the crystallization core lab at deCODE biostructures including Katie Thompkins, Diana Craigen, Laura Law, and Becky Poplawski. We also thank former members our laboratories for their assistance as follows: Denise Connor for help preparing library samples; Thomas Richter for X-ray data collection; Vincent Sandanayaka and Thorkell Andresson for fragment library design. We thank members of the Protein Structure Initiative community including Ian Wilson, Wladek Minor, Ashley Deacon, Marc Elsinger, and Abhinav Kumar for providing calculations on the number of ligand bound structures reported from structural genomics efforts, work that was supported in part by the NIGMS-NCRR cosponsored PSI-2 Specialized Center Grant U54 GM074961 through the Accelerated Technologies Center for Gene to 3D Structure (www.ATCG3D.org).

Supporting Information Available: Nine figures showing property distribution for the FOL library; 3D diversity plot of the FOL library components and the LTA4H hits; binding mode of compound **7** to the surface of LTA4H; comparison of LTA4H binding by dihydroresveratrol (**3**) to compound **4**, benzoxyphenyls (from PDB codes 3CHQ and 3CHO), and a hydroxamic acid (docked to match the reported structures of Thunnissen et al.); thiophene and thaizole ring containing fragments (**7**−**9**) binding into LTA4H L-shaped pocket; acetate coordinating active site Zn^{2+} together with fragments bound; indole structures providing coverage of the benzoxazole and benzthiazoles of Grice et al. and Rao et al.; superposition of LTA4H binding modes of fragments 3−6 compared to Kirkland et al.'s 3CHO and 3CHQ, with docked poses for Grice et al.'s 10a and 10e and Rao et al.'s 26993135; BEI vs SEI plots for fragments and their derivatives; and two tables listing X-ray crystallographic data collection and refinement statistics and comparative IC_{50} data for peptidase, hydrolase, and HWB assays. This material is available free of charge via the Internet at http://pubs.acs.org.

References

(1) Zheng, H.; Chruszcz, M.; Lasota, P.; Lebioda, L.; Minor, W. Data mining of metal ion environments present in protein structures. *J. Inorg. Biochem.* **2008**, *102*, 1765–1776.
(2) Tan, X.; Calderon-Villalobos, L. I.; Sharon, M.; Zheng, C.; Robinson, C. V.; Estelle, M.; Zheng, N. Mechanism of auxin perception by the TIR1 ubiquitin ligase. *Nature* **2007**, *446*, 640–645.
(3) Shimada, A.; Ueguchi-Tanaka, M.; Nakatsu, T.; Nakajima, M.; Naoe, Y.; Ohmiya, H.; Kato, H.; Matsuoka, M. Structural basis for gibberellin recognition by its receptor GID1. *Nature* **2008**, *456*, 520–523.
(4) Kuntz, I. D.; Chen, K.; Sharp, K. A.; Kollman, P. A. The maximal affinity of ligands. *Proc. Natl. Acad. Sci. U.S.A.* **1999**, *96*, 9997–10002.
(5) Wishart, D. S.; Knox, C.; Guo, A. C.; Eisner, R.; Young, N.; Gautam, B.; Hau, D. D.; Psychogios, N.; Dong, E.; Bouatra, S.; Mandal, R.; Sinelnikov, I.; Xia, J.; Jia, L.; Cruz, J. A.; Lim, E.; Sobsey, C. A.; Shrivastava, S.; Huang, P.; Liu, P.; Fang, L.; Peng, J.; Fradette, R.; Cheng, D.; Tzur, D.; Clements, M.; Lewis, A.; De Souza, A.; Zuniga, A.; Dawe, M.; Xiong, Y.; Clive, D.; Greiner, R.; Nazyrova, A.; Shaykhutdinov, R.; Li, L.; Vogel, H. J.; Forsythe, I. HMDB: a knowledgebase for the human metabolome. *Nucleic Acids Res.* **2008**, *37* (Database Issue), D603–D610.
(6) Dobson, P. D.; Patel, Y.; Kell, D. B. "Metabolite-likeness" as a criterion in the design and selection of pharmaceutical drug libraries. *Drug Discovery Today* **2009**, *14*, 31–40.
(7) Karakoc, E.; Sahinalp, S. C.; Cherkasov, A. Comparative QSAR- and fragments distribution analysis of drugs, druglikes, metabolic substances, and antimicrobial compounds. *J. Chem. Inf. Model.* **2006**, *46*, 2167–2182.
(8) Morphy, R.; Rankovic, Z. Fragments, network biology and designing multiple ligands. *Drug Discovery Today* **2007**, *12*, 156–160.
(9) Congreve, M.; Chessari, G.; Tisi, D.; Woodhead, A. J. Recent developments in fragment-based drug discovery. *J. Med. Chem.* **2008**, *51*, 3661–3689.
(10) Rees, D. C.; Congreve, M.; Murray, C. W.; Carr, R. Fragment-based lead discovery. *Nat. Rev. Drug Discovery* **2004**, *3*, 660–672.
(11) Congreve, M.; Carr, R.; Murray, C.; Jhoti, H. A "rule of three" for fragment-based lead discovery?. *Drug Discovery Today* **2003**, *8*, 876–877.
(12) Nienaber, V. L.; Greer, J. Discovering novel ligands for macromolecules using X-ray crystallographic screening. *Nat. Biotechnol.* **2000**, *18*, 1105–1108.
(13) Neumann, T.; Junker, H. D.; Schmidt, K.; Sekul, R. SPR-based fragment screening: advantages and applications. *Curr. Top. Med. Chem.* **2007**, *7*, 1630–1642.
(14) Jhoti, H.; Cleasby, A.; Verdonk, M.; Williams, G. Fragment-based screening using X-ray crystallography and NMR spectroscopy. *Curr. Opin. Chem. Biol.* **2007**, *11*, 485–493.

(15) Erlanson, D. A. Fragment-based lead discovery: a chemical update. *Curr. Opin. Biotechnol.* **2006**, *17*, 643–652.
(16) Abad-Zapatero, C.; Metz, J. T. Ligand efficiency indices as guideposts for drug discovery. *Drug Discovery Today* **2005**, *10*, 464–469.
(17) Makara, G. M. On sampling of fragment space. *J. Med. Chem.* **2007**, *50*, 3214–3221.
(18) Bemis, G. W.; Murcko, M. A. The properties of known drugs. 1. Molecular frameworks. *J. Med. Chem.* **1996**, *39*, 2887–2893.
(19) Duarte, C. D.; Barreiro, E. J.; Fraga, C. A. Privileged structures: a useful concept for the rational design of new lead drug candidates. *Mini-Rev. Med. Chem.* **2007**, *7*, 1108–1119.
(20) Muller, G. Medicinal chemistry of target family-directed masterkeys. *Drug Discovery Today* **2003**, *8*, 681–691.
(21) Siegel, M. G.; Vieth, M. Drugs in other drugs: a new look at drugs as fragments. *Drug Discovery Today* **2007**, *12*, 71–79.
(22) Smith, E.; Morowitz, H. J. Universality in intermediary metabolism. *Proc. Natl. Acad. Sci. U.S.A.* **2004**, *101*, 13168–13173.
(23) Binkowski, T. A.; Joachimiak, A. Protein functional surfaces: global shape matching and local spatial alignments of ligand binding sites. *BMC Struct. Biol.* **2008**, *8*, 45.
(24) Lipkus, A. H.; Yuan, Q.; Lucas, K. A.; Funk, S. A.; Bartelt, W. F. 3rd; Schenck, R. J.; Trippe, A. J. Structural diversity of organic chemistry. A scaffold analysis of the CAS Registry. *J. Org. Chem.* **2008**, *73*, 4443–4451.
(25) Kull, F.; Ohlson, E.; Haeggstrom, J. Z. Cloning and characterization of a bifunctional leukotriene A(4) hydrolase from *Saccharomyces cerevisiae*. *J. Biol. Chem.* **1999**, *274*, 34683–34690.
(26) Thunnissen, M. M.; Nordlund, P.; Haeggstrom, J. Z. Crystal structure of human leukotriene A(4) hydrolase, a bifunctional enzyme in inflammation. *Nat. Struct. Biol.* **2001**, *8*, 131–135.
(27) Tholander, F.; Muroya, A.; Roques, B. P.; Fournie-Zaluski, M. C.; Thunnissen, M. M.; Haeggstrom, J. Z. Structure-based dissection of the active site chemistry of leukotriene A4 hydrolase: implications for M1 aminopeptidases and inhibitor design. *Chem. Biol.* **2008**, *15*, 920–929.
(28) Qiu, H.; Gabrielsen, A.; Agardh, H. E.; Wan, M.; Wetterholm, A.; Wong, C. H.; Hedin, U.; Swedenborg, J.; Hansson, G. K.; Samuelsson, B.; Paulsson-Berne, G.; Haeggstrom, J. Z. Expression of 5-lipoxygenase and leukotriene A4 hydrolase in human atherosclerotic lesions correlates wtih symptoms of plaque instability. *Proc. Natl. Acad. Sci. U.S.A.* **2006**, *103*, 8161–8166.
(29) Helgadottir, A.; Manolescu, A.; Helgason, A.; Thorleifsson, G.; Thorsteinsdottir, U.; Gudbjartsson, D. F.; Gretarsdottir, S.; Magnusson, K. P.; Gudmundsson, G.; Hicks, A.; Jonsson, T.; Grant, S. F.; Sainz, J.; O'Brien, S. J.; Sveinbjornsdottir, S.; Valdimarsson, E. M.; Matthiasson, S. E.; Levey, A. I.; Abramson, J. L.; Reilly, M. P.; Vaccarino, V.; Wolfe, M. L.; Gudnason, V.; Quyyumi, A. A.; Topol, E. J.; Rader, D. J.; Thorgeirsson, G.; Gulcher, J. R.; Hakonarson, H.; Kong, A.; Stefansson, K. A variant of the gene encoding leukotriene A4 hydrolase confers ethnicity-specific risk of myocardial infarction. *Nat. Genet.* **2006**, *38*, 68–74.
(30) Sanchez-Galan, E.; Gomez-Hernandez, A.; Vidal, C.; Martin-Ventura, J. L.; Blanco-Colio, L. M.; Munoz-Garcia, B.; Ortega, L.; Egido, J.; Tunon, J. Leukotriene B4 enhances the activity of nuclear factor-kappaB pathway through BLT1 and BLT2 receptors in atherosclerosis. *Cardiovasc. Res.* **2009**, *81*, 216–225.
(31) Holloway, J. W.; Barton, S. J.; Holgate, S. T.; Rose-Zerilli, M. J.; Sayers, I. The role of LTA4H and ALOX5AP polymorphism in asthma and allergy susceptibility. *Allergy* **2008**, *63*, 1036–1053.
(32) Penning, T. D.; Chandrakumar, N. S.; Desai, B. N.; Djuric, S. W.; Gasiecki, A. F.; Malecha, J. W.; Miyashiro, J. M.; Russell, M. A.; Askonas, L. J.; Gierse, J. K.; Harding, E. I.; Highkin, M. K.; Kachur, J. F.; Kim, S. H.; Villani-Price, D.; Pyla, E. Y.; Ghoreishi-Haack, N. S.; Smith, W. G. Synthesis of imidazopyridines and purines as potent inhibitors of leukotriene A4 hydrolase. *Bioorg. Med. Chem. Lett.* **2003**, *13*, 1137–1139.
(33) Penning, T. D.; Chandrakumar, N. S.; Desai, B. N.; Djuric, S. W.; Gasiecki, A. F.; Liang, C. D.; Miyashiro, J. M.; Russell, M. A.; Askonas, L. J.; Gierse, J. K.; Harding, E. I.; Highkin, M. K.; Kachur, J. F.; Kim, S. H.; Villani-Price, D.; Pyla, E. Y.; Ghoreishi-Haack, N. S.; Smith, W. G. Pyrrolidine and piperidine analogues of SC-57461A as potent, orally active inhibitors of leukotriene A(4) hydrolase. *Bioorg. Med. Chem. Lett.* **2002**, *12*, 3383–3386.
(34) Penning, T. D.; Chandrakumar, N. S.; Chen, B. B.; Chen, H. Y.; Desai, B. N.; Djuric, S. W.; Docter, S. H.; Gasiecki, A. F.; Haack, R. A.; Miyashiro, J. M.; Russell, M. A.; Yu, S. S.; Corley, D. G.; Durley, R. C.; Kilpatrick, B. F.; Parnas, B. L.; Askonas, L. J.; Gierse, J. K.; Harding, E. I.; Highkin, M. K.; Kachur, J. F.; Kim, S. H.; Krivi, G. G.; Villani-Price, D.; Pyla, E. Y.; Smith, W. G. Structure−activity relationship studies on 1-[2-(4-phenylphenoxy)ethyl]pyrrolidine (SC-22716), a potent inhibitor of leukotriene A(4) (LTA(4)) hydrolase. *J. Med. Chem.* **2000**, *43*, 721–735.
(35) Djuric, S. W.; Huff, R. M.; Penning, T. D.; Clare, M.; Swenton, L.; Kachur, J. F.; Villani-Price, D.; Krivi, G. G.; Pyla, E. Y.; Warren, T. G. Synthesis and pharmacological activity of rationally designed inhibitors of the leukotriene A4 hydrolase enzyme. *Bioorg. Med. Chem.* **1992**, *2*, 1367–1370.
(36) Fretland, D. J.; Anglin, C. P.; Bremer, M.; Isakson, P.; Widomski, D. L.; Paulson, S. K.; Docter, S. H.; Djuric, S. W.; Penning, T. D.; Yu, S. Antiinflammatory effects of second-generation leukotriene B4 receptor antagonist, SC-53228: impact upon leukotriene B4- and 12(R)-HETE-mediated events. *Inflammation* **1995**, *19*, 193–205.
(37) Penning, T. D.; Djuric, S. W.; Miyashiro, J. M.; Yu, S.; Snyder, J. P.; Spangler, D.; Anglin, C. P.; Fretland, D. J.; Kachur, J. F.; Keith, R. H.; et al. Second-generation leukotriene B4 receptor antagonists related to SC-41930: heterocyclic replacement of the methyl ketone pharmacophore. *J. Med. Chem.* **1995**, *38*, 858–868.
(38) Penning, T. D.; Djuric, S. W.; Docter, S. H.; Yu, S. S.; Spangler, D.; Anglin, C. P.; Fretland, D. J.; Kachur, J. F.; Keith, R. H.; Tsai, B. S. The design and synthesis of second generation leukotriene B4 (LTB4) receptor antagonists related to SC-41930. *Agents Actions* **1993**, *39 Spec. No*., C11–C13.
(39) Grice, C. A.; Tays, K. L.; Savall, B. M.; Wei, J.; Butler, C. R.; Axe, F. U.; Bembenek, S. D.; Fourie, A. M.; Dunford, P. J.; Lundeen, K.; Coles, F.; Xue, X.; Riley, J. P.; Williams, K. N.; Karlsson, L.; Edwards, J. P. Identification of a potent, selective, and orally active leukotriene A4 hydrolase inhibitor with anti-inflammatory activity. *J. Med. Chem.* **2008**, *51*, 4150–4169.
(40) Kirkland, T. A.; Adler, M.; Bauman, J. G.; Chen, M.; Haeggstrom, J. Z.; King, B.; Kochanny, M. J.; Liang, A. M.; Mendoza, L.; Phillips, G. B.; Thunnissen, M.; Trinh, L.; Whitlow, M.; Ye, B.; Ye, H.; Parkinson, J.; Guilford, W. J. Synthesis of glutamic acid analogs as potent inhibitors of leukotriene A4 hydrolase. *Bioorg. Med. Chem.* **2008**, *16*, 4963–4983.
(41) Ye, B.; Bauman, J.; Chen, M.; Davey, D.; Khim, S. K.; King, B.; Kirkland, T.; Kochanny, M.; Liang, A.; Lentz, D.; May, K.; Mendoza, L.; Phillips, G.; Selchau, V.; Schlyer, S.; Tseng, J. L.; Wei, R. G.; Ye, H.; Parkinson, J.; Guilford, W. J. Synthesis of *N*-alkyl glycine amides as potent inhibitors of leukotriene A4 hydrolase. *Bioorg. Med. Chem. Lett.* **2008**, *18*, 3891–3894.
(42) Khim, S. K.; Bauman, J.; Evans, J.; Freeman, B.; King, B.; Kirkland, T.; Kochanny, M.; Lentz, D.; Liang, A.; Mendoza, L.; Phillips, G.; Tseng, J. L.; Wei, R. G.; Ye, H.; Yu, L.; Parkinson, J.; Guilford, W. J. Discovery of novel and potent aryl diamines as leukotriene A4 hydrolase inhibitors. *Bioorg. Med. Chem. Lett.* **2008**, *18*, 3895–3898.
(43) Sandanayaka, V.; Mamat, B.; Mishra, R. K.; Winger, J.; Krohn, M.; Zhao, L.-M.; Kevan, M.; Enache, L.; D., S.; Onua, E.; Zhang, J.; Halldorsdottir, G.; Sigthorsdottir, H.; Thorlaksdottir, A.; Sigthorsson, G.; Thorsteinnsdottir, M.; Davies, D. R.; Stewart, L. J.; Zembower, D. E.; Andresson, T.; Kiselyov, A. S.; Singh, J.; Gurney, M. E. Discovery of DG-051 as a novel leukotriene A4 hydrolase inhibitor of leukotriene B4 biosynthesis. Unpublished results, **2009**.
(44) Schorlemmer, H. U.; Bosslet, K.; Dickneite, G.; Luben, G.; Sedlacek, H. H. Studies on the mechanisms of action of the immunomodulator bestatin in various screening test systems. *Behring Inst. Mitt.* **1984**, 157–173.
(45) Tholander, F.; Kull, F.; Ohlson, E.; Shafqat, J.; Thunnissen, M. M.; Haeggstrom, J. Z. Leukotriene A4 hydrolase, insights into the molecular evolution by homology modeling and mutational analysis of enzyme from *Saccharomyces cerevisiae*. *J. Biol. Chem.* **2005**, *280*, 33477–33486.
(46) Haeggstrom, J. Z. Leukotriene A4 hydrolase/aminopeptidase, the gatekeeper of chemotactic leukotriene B4 biosynthesis. *J. Biol. Chem.* **2004**, *279*, 50639–50642.
(47) Yokomizo, T.; Kato, K.; Terawaki, K.; Izumi, T.; Shimizu, T. A second leukotriene B(4) receptor, BLT2. A new therapeutic target in inflammation and immunological disorders. *J. Exp. Med.* **2000**, *192*, 421–432.
(48) Yokomizo, T.; Izumi, T.; Chang, K.; Takuwa, Y.; Shimizu, T. A G-Protein-coupled receptor for leukotriene B4 that mediates chemotaxis. *Nature* **1997**, *387*, 620–624.
(49) Tryselius, Y.; Nilsson, N. E.; Kotarsky, K.; Olde, B.; Owman, C. Cloning and characterization of cDNA encoding a novel human leukotriene B(4) receptor. *Biochem. Biophys. Res. Commun.* **2000**, *274*, 377–382.
(50) Kamohara, M.; Takasaki, J.; Matsumoto, M.; Saito, T.; Ohishi, T.; Ishii, H.; Furuichi, K. Molecular cloning and characterization of another leukotriene B4 receptor. *J. Biol. Chem.* **2000**, *275*, 27000–27004.
(51) Lundeen, K. A.; Sun, B.; Karlsson, L.; Fourie, A. M. Leukotriene B4 receptors BLT1 and BLT2: expression and function in human and murine mast cells. *J. Immunol.* **2006**, *177*, 3439–3447.

(52) Bohacek, R. S.; Dalgarno, D. C.; Hatada, M.; Jacobsen, V. A.; Lynch, B. A.; Macek, K. J.; Merry, T.; Metcalf, C. A. 3rd; Narula, S. S.; Sawyer, T. K.; Shakespeare, W. C.; Violette, S. M.; Weigele, M. X-ray structure of citrate bound to Src SH2 leads to a high-affinity, bone-targeted Src SH2 inhibitor. *J. Med. Chem.* **2001**, *44*, 660–663.
(53) Kwong, P. D.; Wyatt, R.; Majeed, S.; Robinson, J.; Sweet, R. W.; Sodroski, J.; Hendrickson, W. A. Structures of HIV-1 gp120 envelope glycoproteins from laboratory-adapted and primary isolates. *Structure* **2000**, *8*, 1329–1339.
(54) Macbeth, M. R.; Schubert, H. L.; Vandemark, A. P.; Lingam, A. T.; Hill, C. P.; Bass, B. L. Inositol hexakisphosphate is bound in the ADAR2 core and required for RNA editing. *Science* **2005**, *309*, 1534–1539.
(55) Jensen, R. A. Enzyme recruitment in evolution of new function. *Annu. Rev. Microbiol.* **1976**, *30*, 409–425.
(56) Khersonsky, O.; Roodveldt, C.; Tawfik, D. S. Enzyme promiscuity: evolutionary and mechanistic aspects. *Curr. Opin. Chem. Biol.* **2006**, *10*, 498–508.
(57) O'Brien, P. J.; Herschlag, D. Catalytic promiscuity and the evolution of new enzymatic activities. *Chem. Biol.* **1999**, *6*, R91–R105.
(58) Joerger, A. C.; Mayer, S.; Fersht, A. R. Mimicking natural evolution in vitro: an *N*-acetylneuraminate lyase mutant with an increased dihydrodipicolinate synthase activity. *Proc. Natl. Acad. Sci. U.S.A.* **2003**, *100*, 5694–5699.
(59) Saraogi, I.; Hamilton, A. D. alpha-Helix mimetics as inhibitors of protein−protein interactions. *Biochem. Soc. Trans.* **2008**, *36*, 1414–1417.
(60) Biros, S. M.; Moisan, L.; Mann, E.; Carella, A.; Zhai, D.; Reed, J. C.; Rebek, J. Jr. Heterocyclic alpha-helix mimetics for targeting protein−protein interactions. *Bioorg. Med. Chem. Lett.* **2007**, *17*, 4641–4645.
(61) Robinson, J. A. Beta-hairpin peptidomimetics: design, structures and biological activities. *Acc. Chem. Res.* **2008**, *41*, 1278–1288.
(62) Jang, M.; Cai, L.; Udeani, G. O.; Slowing, K. V.; Thomas, C. F.; Beecher, C. W.; Fong, H. H.; Farnsworth, N. R.; Kinghorn, A. D.; Mehta, R. G.; Moon, R. C.; Pezzuto, J. M. Cancer chemopreventive activity of resveratrol, a natural product derived from grapes. *Science* **1997**, *275*, 218–220.
(63) Jayatilake, G. S.; Jayasuriya, H.; Lee, E. S.; Koonchanok, N. M.; Geahlen, R. L.; Ashendel, C. L.; McLaughlin, J. L.; Chang, C. J. Kinase inhibitors from *Polygonum cuspidatum*. *J. Nat. Prod.* **1993**, *56*, 1805–1810.
(64) Wang, Z.; Huang, Y.; Zou, J.; Cao, K.; Xu, Y.; Wu, J. M. Effects of red wine and polyphenol resveratrol on platelet aggregation in vivo and in vitro. *Int. J. Mol. Med.* **2002**, *9*, 77–79.
(65) Orallo, F.; Alvarez, E.; Camina, M.; Leiro, J. M.; Gomez, E.; Fernandez, P. The possible implication of trans-resveratrol in the cardioprotective effects of long-term moderate wine consumption. *Mol. Pharmacol.* **2002**, *61*, 294–302.
(66) Bhat, K. P. L.; Kosmeder, J. W. n.; Pezzuto, J. M. Biological effects of resveratrol. *Antioxid. Redox Signaling* **2001**, *3*, 1041–1064.
(67) Kopp, P. Resveratrol, a phytoestrogen found in red wine. A possible explanation for the conundrum of the "French paradox"?. *Eur. J. Endocrinol.* **1998**, *138*, 619–620.
(68) Adams, M.; Pacher, T.; Greger, H.; Bauer, R. Inhibition of leukotriene biosynthesis by stilbenoids from Stemona species. *J. Nat. Prod.* **2005**, *68*, 83–85.
(69) Baur, J. A.; Pearson, K. J.; Price, N. L.; Jamieson, H. A.; Lerin, C.; Kalra, A.; Prabhu, V. V.; Allard, J. S.; Lopez-Lluch, G.; Lewis, K.; Pistell, P. J.; Poosala, S.; Becker, K. G.; Boss, O.; Gwinn, D.; Wang, M.; Ramaswamy, S.; Fishbein, K. W.; Spencer, R. G.; Lakatta, E. G.; Le Couteur, D.; Shaw, R. J.; Navas, P.; Puigserver, P.; Ingram, D. K.; de Cabo, R.; Sinclair, D. A. Resveratrol improves health and survival of mice on a high-calorie diet. *Nature* **2006**, *444*, 337–342.
(70) Baur, J. A.; Sinclair, D. A. Therapeutic potential of resveratrol: the in vivo evidence. *Nat. Rev. Drug Discovery* **2006**, *5*, 493–506.
(71) Walle, T.; Hsieh, F.; DeLegge, M. H.; Oatis, J. E. Jr.; Walle, U. K. High absorption but very low bioavailability of oral resveratrol in humans. *Drug Metab. Dispos.* **2004**, *32*, 1377–1382.
(72) Wenzel, E.; Somoza, V. Metabolism and bioavailability of trans-resveratrol. *Mol. Nutr. Food Res.* **2005**, *49*, 472–481.
(73) Thunnissen, M. M.; Andersson, B.; Samuelsson, B.; Wong, C. H.; Haeggstrom, J. Z. Crystal structures of leukotriene A4 hydrolase in complex with captopril and two competitive tight-binding inhibitors. *FASEB J.* **2002**, *16*, 1648–1650.
(74) McGovern, S. L.; Caselli, E.; Grigorieff, N.; Shoichet, B. K. A common mechanism underlying promiscuous inhibitors from virtual and high-throughput screening. *J. Med. Chem.* **2002**, *45*, 1712–1722.
(75) Meyer, B.; Peters, T. NMR spectroscopy techniques for screening and identifying ligand binding to protein receptors. *Angew. Chem., Int. Ed.* **2003**, *42*, 864–90.
(76) Gorczynski, M. J.; Grembecka, J.; Zhou, Y.; Kong, Y.; Roudaia, L.; Douvas, M. G.; Newman, M.; Bielnicka, I.; Baber, G.; Corpora, T.; Shi, J.; Sridharan, M.; Lilien, R.; Donald, B. R.; Speck, N. A.; Brown, M. L.; Bushweller, J. H. Allosteric inhibition of the protein−protein interaction between the leukemia-associated proteins Runx1 and CBFbeta. *Chem. Biol.* **2007**, *14*, 1186–1197.
(77) Hajduk, P. J. Fragment-based drug design: how big is too big?. *J. Med. Chem.* **2006**, *49*, 6972–6976.
(78) Szczepankiewicz, B. G.; Liu, G.; Hajduk, P. J.; Abad-Zapatero, C.; Pei, Z.; Xin, Z.; Lubben, T. H.; Trevillyan, J. M.; Stashko, M. A.; Ballaron, S. J.; Liang, H.; Huang, F.; Hutchins, C. W.; Fesik, S. W.; Jirousek, M. R. Discovery of a potent, selective protein tyrosine phosphatase 1B inhibitor using a linked-fragment strategy. *J. Am. Chem. Soc.* **2003**, *125*, 4087–4096.
(79) Lesuisse, D.; Lange, G.; Deprez, P.; Benard, D.; Schoot, B.; Delettre, G.; Marguette, J. P.; Broto, P.; Jean-Baptiste, V.; Sarubbi, E.; Mandine, E. SAR and X-ray. A new approach combining fragment-based screening and rational drug design: application to the discovery of nanomolar inhibitors of Src SH2. *J. Med. Chem.* **2002**, *45*, 2379–2387.
(80) Shuker, S. B.; Hajduk, P. J.; Meadows, R. P.; Fesik, S. W. Discovering high-affinity ligands for proteins: SAR by NMR. *Science* **1996**, *274*, 1531–1534.
(81) Oltersdorf, T.; Elmore, S. W.; Shoemaker, A. R.; Armstrong, R. C.; Augeri, D. J.; Belli, B. A.; Bruncko, M.; Deckwerth, T. L.; Dinges, J.; Hajduk, P. J.; Joseph, M. K.; Kitada, S.; Korsmeyer, S. J.; Kunzer, A. R.; Letai, A.; Li, C.; Mitten, M. J.; Nettesheim, D. G.; Ng, S.; Nimmer, P. M.; O'Connor, J. M.; Oleksijew, A.; Petros, A. M.; Reed, J. C.; Shen, W.; Tahir, S. K.; Thompson, C. B.; Tomaselli, K. J.; Wang, B.; Wendt, M. D.; Zhang, H.; Fesik, S. W.; Rosenberg, S. H. An inhibitor of Bcl-2 family proteins induces regression of solid tumours. *Nature* **2005**, *435*, 677–681.
(82) Pennazio, S. The discovery of the chemical nature of the plant hormone auxin. *Riv. Biol.* **2002**, *95*, 289–308.
(83) Minderaa, R. B.; Anderson, G. M.; Volkmar, F. R.; Akkerhuis, G. W.; Cohen, D. J. Urinary 5-hydroxyindoleacetic acid and whole blood serotonin and tryptophan in autistic and normal subjects. *Biol. Psychiatry* **1987**, *22*, 933–940.
(84) Goodey, N. M.; Benkovic, S. J. Allosteric regulation and catalysis emerge via a common route. *Nat. Chem. Biol.* **2008**, *4*, 474–482.
(85) Milne, J. C.; Denu, J. M. The Sirtuin family: therapeutic targets to treat diseases of aging. *Curr. Opin. Chem. Biol.* **2008**, *12*, 11–17.
(86) Milne, J. C.; Lambert, P. D.; Schenk, S.; Carney, D. P.; Smith, J. J.; Gagne, D. J.; Jin, L.; Boss, O.; Perni, R. B.; Vu, C. B.; Bemis, J. E.; Xie, R.; Disch, J. S.; Ng, P. Y.; Nunes, J. J.; Lynch, A. V.; Yang, H.; Galonek, H.; Israelian, K.; Choy, W.; Iffland, A.; Lavu, S.; Medvedik, O.; Sinclair, D. A.; Olefsky, J. M.; Jirousek, M. R.; Elliott, P. J.; Westphal, C. H. Small molecule activators of SIRT1 as therapeutics for the treatment of type 2 diabetes. *Nature* **2007**, *450*, 712–716.
(87) Lavu, S.; Boss, O.; Elliott, P. J.; Lambert, P. D. Sirtuins—novel therapeutic targets to treat age-associated diseases. *Nat. Rev. Drug Discovery* **2008**, *7*, 841–853.
(88) Rao, N. L.; Dunford, P. J.; Xue, X.; Jiang, X.; Lundeen, K. A.; Coles, F.; Riley, J. P.; Williams, K. N.; Grice, C. A.; Edwards, J. P.; Karlsson, L.; Fourie, A. M. Anti-inflammatory activity of a potent, selective leukotriene A4 hydrolase inhibitor in comparison with the 5-lipoxygenase inhibitor zileuton. *J. Pharmacol. Exp. Ther.* **2007**, *321*, 1154–1160.
(89) Meierhenrich, U. J.; Munoz Caro, G. M.; Bredehoft, J. H.; Jessberger, E. K.; Thiemann, W. H. Identification of diamino acids in the Murchison meteorite. *Proc. Natl. Acad. Sci. U.S.A.* **2004**, *101*, 9182–9186.
(90) Llorca, J. Organic matter in meteorites. *Int. Microbiol.* **2004**, *7*, 239–248.
(91) Morowitz, H. J.; Kostelnik, J. D.; Yang, J.; Cody, G. D. The origin of intermediary metabolism. *Proc. Natl. Acad. Sci. U.S.A.* **2000**, *97*, 7704–7708.
(92) Hann, M. M.; Oprea, T. I. Pursuing the leadlikeness concept in pharmaceutical research. *Curr. Opin. Chem. Biol.* **2004**, *8*, 255–263.
(93) Davis, J. M.; Tsou, L. K.; Hamilton, A. D. Synthetic non-peptide mimetics of alpha-helices. *Chem. Soc. Rev.* **2007**, *36*, 326–334.
(94) Verlinde, C. L. M. J.; Kim, H.; Bernstein, B. E.; Mande, S. C.; Hol, W. G. Antitrypanosomiasis Drug Development Based on Structures of Glycolytic Enzymes. In *Structure-Based Drug Design*; Veerapandian, P., Ed.; Marcel Dekker: New York, 1997; pp 365−394.
(95) Bosch, J.; Robien, M. A.; Mehlin, C.; Boni, E.; Riechers, A.; Buckner, F. S.; Van Voorhis, W. C.; Myler, P. J.; Worthey, E. A.; DeTitta, G.; Luft, J. R.; Lauricella, A.; Gulde, S.; Anderson, L. A.; Kalyuzhniy, O.; Neely, H. M.; Ross, J.; Earnest, T. N.; Soltis, M.; Schoenfeld, L.; Zucker, F.; Merritt, E. A.; Fan, E.; Verlinde, C. L. M. J.; Hol, W. G. Using fragment cocktail crystallography to

assist inhibitor design of *Trypanosoma brucei* nucleoside 2-deoxyribosyltransferase. *J. Med. Chem.* **2006**, *49*, 5939–5946.
(96) Jain, A. N. Surflex: fully automatic flexible molecular docking using a molecular similarity-based search engine. *J. Med. Chem.* **2003**, *46*, 499–511.
(97) Welch, W.; Ruppert, J.; Jain, A. N. Hammerhead: fast, fully automated docking of flexible ligands to protein binding sites. *Chem. Biol.* **1996**, *3*, 449–462.
(98) Costantino, L.; Barlocco, D. Privileged structures as leads in medicinal chemistry. *Curr. Med. Chem.* **2006**, *13*, 65–85.